2012

# Integrated Fiber Electrospinning: Creating Spatially Complex Electrospun Scaffolds With Minimal Delamination

Casey Grey
*Virginia Commonwealth University*

# INTEGRATED FIBER ELECTROSPINNING: CREATING SPATIALLY COMPLEX ELECTROSPUN SCAFFOLDS WITH MINIMAL DELAMINATION

A thesis submitted in partial fulfillment of the requirements for the degree of Master of Science at Virginia Commonwealth University

by

CASEY GREY
B.S., Virginia Military Institute, Lexington, Virginia
2007

Director: DAVID SIMPSON, PH.D.
Associate Professor, Department of Anatomy and Neurobiology

Co-Director: GARY BOWLIN, PH.D.
Professor, Department of Biomedical Engineering

Virginia Commonwealth University
Richmond, Virginia
August, 2012

Acknowledgement

I would like to thank Dr. David Simpson for his support, guidance, and humor throughout my time in his lab. Thanks so much to Dr. Balendu Shekhar Jha and Dr. Rusty Bowman for their help and collaboration. I would also like to thank Dr. Gary Bowlin and his graduate students for the use of his equipment and the guidance they offered. Thanks to Scott Newton for his tireless work (especially on fiber counts).

I would like to recognize that Scanning Electron Microscopy was performed at the Virginia Commonwealth University Department of Anatomy and Neurobiology Microscopy Facility, supported, in part, with funding from NIH-NINDS Center core grant 5P30NS047463 and NIH-NCRR grant 1S10RR022495.

Finally I would like to dedicate this thesis to my family for their incredible love and support. I can't put into words what they mean to me and how much they've helped along the way.

Table of Contents

**Abstract**

INTEGRATED FIBER ELECTROSPINNING: CREATING SPATIALLY COMPLEX ELECTROSPUN SCAFFOLDS WITH MINIMAL DELAMINATION

By Casey Paul Grey, B.S. Mechanical Engineering

A thesis submitted in partial fulfillment of the requirements for the degree of Master of Science at Virginia Commonwealth University.

Virginia Commonwealth University, 2012.

Major Director: DAVID SIMPSON, PH.D.
Associate Professor, Department of Anatomy and Neurobiology

Tissue engineering scaffolds come in many shapes and sizes, however, due to difficulty manufacturing the microstructure architecture required in tissue engineering, most scaffolds are architecturally non-dynamic in nature. Because the microstructural architecture of all biological tissues is inherently complicated, non-dynamic tissue engineering scaffolds tend to be a poor platform for tissue regeneration. The current method for manufacturing dynamic tissue engineering scaffolds involves electrospinning successive layers of different fibers, an approach that exhibits no fiber transition between layers and subsequent delamination problems. In this study we aim to address the design challenges of tissue engineering scaffolds through our novel integrated fiber electrospinning technique. Developed in our lab, this electrospinning technique makes it possible to manufacture complex electrospun scaffolds tailorable to

specific tissue engineering needs while minimizing delamination tendencies. Our goal is to enhance the capabilities of the tissue engineering field by increasing the manufacturable scaffold complexity and overall structural integrity of electrospun scaffolds.

# Chapter 1

# Introduction

## 1.1 Background

Tissue engineering scaffolds are biocompatible structures intended to serve either as platforms for tissue regeneration or as functional replacements for damaged tissue [10]. These scaffolds are produced in a variety of ways but typically involve a complex microstructure tailored to a specific tissue engineering application. While current technology in tissue engineering has experienced some success in tissue regrowth and replacement, scaffolds remain either one-dimensional or complex but structurally unsound (specifically layered scaffolds are susceptible to delamination). Our goal is to create a complex tissue engineering scaffold that maintains acceptable mechanical properties through a novel electrospinning technique called “Integrated Fiber Electrospinning.”

Biological systems rarely involve single individual layers, rather they incorporate multiple layers working in synchrony. Blood vessels, for example, incorporate several distinct layers into a unified structure designed specifically to transport blood while withstanding the stresses of vascular loading (Figures 1 and 2).

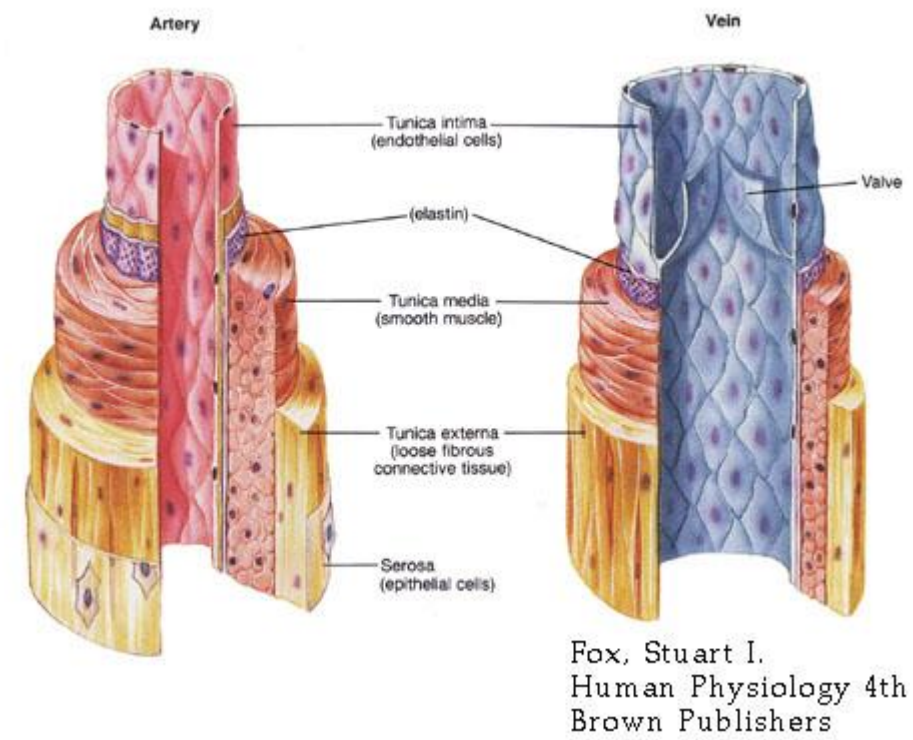


Fig. 1 Blood vessel diagram.

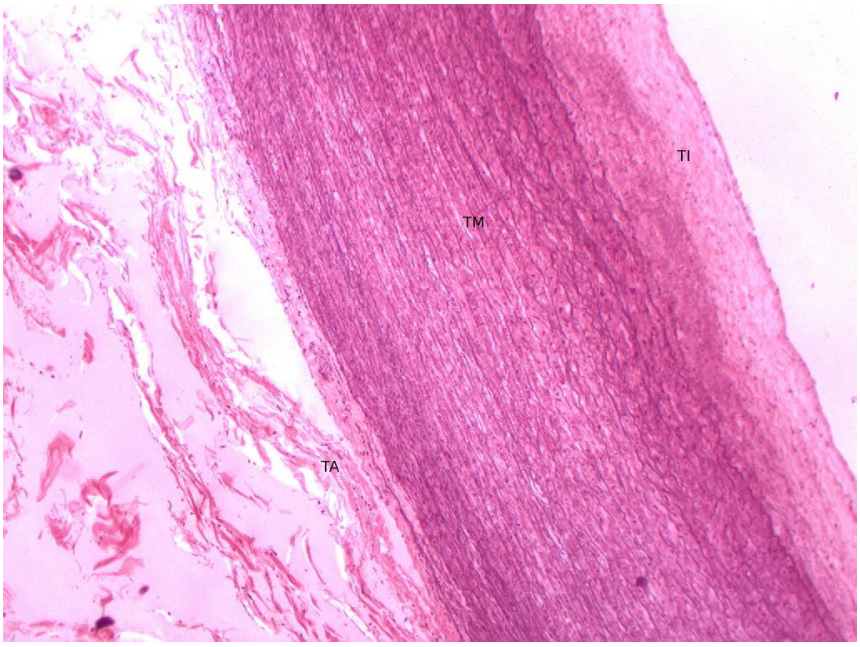


Fig. 2 Arterial micrograph [8], TI) tunica intima, TM) tunica media, TA) tunica adventitia.

Success in tissue engineering is based on many factors, arguably the most important is designing scaffolds to mimic the architectural design in the target natural tissue [7]. It is, in fact, the goal of tissue engineering to manufacture a scaffold that perfectly emulates normal biological tissue so that, when cells are introduced, they grow and respond in the structure as if they were in the natural tissue itself. Achieving this would allow for the replication and replacement of any damaged tissue. While this seems conceptually straightforward the unforgivingly small and specific structural characteristics of individual layers of biological tissue are extremely difficult to replicate. Truthfully, current technology is only moderately successful at creating scaffolds designed for a specific type of tissue. Trying to incorporate several integrated layers into the graft makes the process complexity increase dramatically. The present solution to manufacturing artificial layered structures such as blood vessels is to electrospin different fiber layers in series so that the final scaffold is a laminated construct consisting of different fiber types, each meant to replicate their target tissue layer. The primary problem with this approach is the creation of a laminated structure with no transition between layers. The lack of mechanical communication in laminated structures introduces the risk of delamination failure. This type of failure occurs either because mechanical stress becomes concentrated at the borders or because of differences in material properties such that part of the scaffold is unable to withstand the test conditions. Additionally we question the ability of physiological communication across an abrupt change in fiber size, identity or morphology.

This study focuses on the issue at hand; a true tissue engineering scaffold needs to possess dynamic spatial fiber characteristics while retaining whole scaffold structure properties suitable for withstanding physiological stresses. The design challenge is to create a scaffold that displays unique and dynamic spatial fiber morphology that can communicate load and physiological growth between layers so as to encourage simultaneous tissue growth while mitigating delamination. Because no electrospinning method exists to accomplish this, our approach was to create a new electrospinning technique called Integrated Fiber Electrospinning where the different fibrous layers are joined by controlled transitions, thus allowing for physiological and mechanical communication.

The central hypothesis of this study states that the mechanical properties of a multi-layered structure composed of different fiber sizes can be integrated by incrementally varying the size of the fibers across the cross-sectional length of an electrospun scaffold.

### 1.2 Introduction to Conventional Electrospinning

Electrospinning is a technique that produces a fibrous scaffold from a liquid or a melt solution. The fibers produced from electrospinning can range from about 3 nm to several microns in diameter [1, 3]. These fiber dimensions mimic the fiber sizes encountered within the native extracellular matrix of many organs and tissues. The unique ability of electrospinning to produce fibers on this scale has led to the extensive exploration of this fabrication method for the production of tissue engineering scaffolds using native proteins, synthetic polymers, and blends of natural and synthetic material.

In electrospinning a high voltage power source, typically on the order of 10 to 25 kV, is placed in contact with an electrospinning solution. The charged electrospinning solution is then forced out of a capillary tip, typically a blunted needle tip, towards a grounded target (Figure 3).

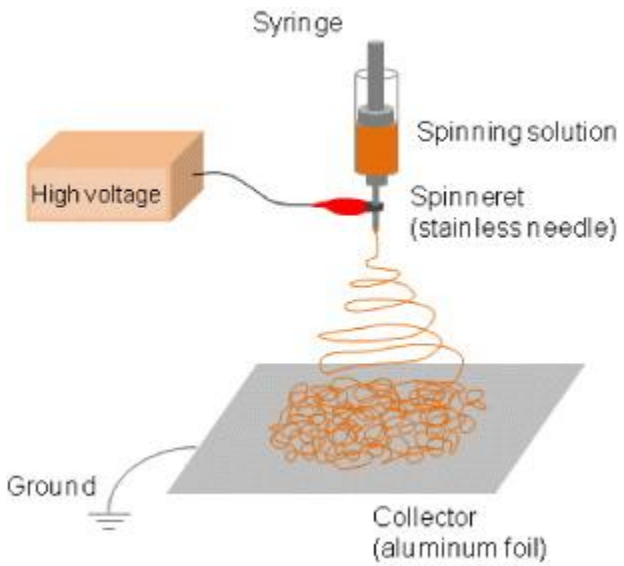


Fig. 3 General electrospinning schematic.

Under the proper conditions, as the electrospinning fluid is forced out of the capillary tip the charge density increases until a Taylor cone forms from which a stream of highly charged electrospinning fluid erupts, traveling towards the target.

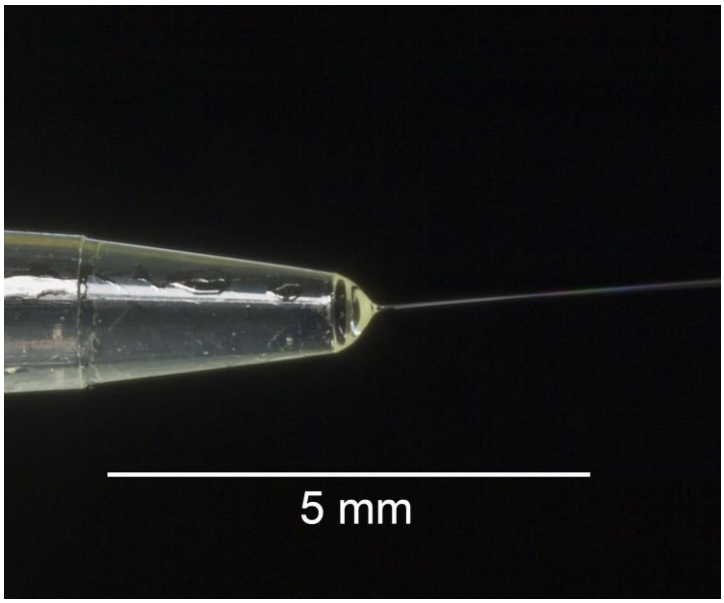


Fig. 4 The Taylor cone is an electrohydrodynamic phenomenon of a charged fluid [11].

This entire process can be divided into four stages: 1) jet initiation; 2) bending instability; 3) solidification of the fiber (solvent evaporation) [1]; and 4) fiber collection. The following segments will discuss these steps in greater detail.

*Jet Initiation*

Speranza et. al. described how the application of an electric field to fluids being ejected from a nozzle create unique electrohydrodynamic properties of the stream. The ejected fluid possesses two functional modes, dripping and jet, depending on the properties of the fluid and the electrical characteristics of the system. At low flow rates and low electrical potentials the fluid forms individual drops (Figure 5). By applying increasingly higher electrical potentials to the fluid the dripping frequency increases until a critical electrical potential is reached where the electrical forces overcome the forces associated with surface tension and the drops transition into a stable jet (Figure 4).

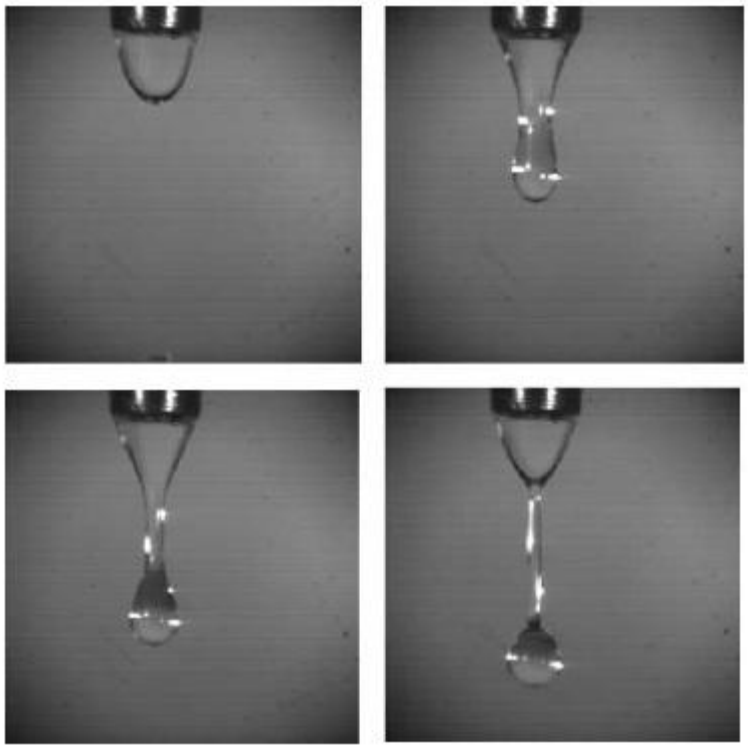

Fig. 5  Formation of drops in an electrospraying situation (8 kV) [4].

Figure 6 shows the relationship between operating voltage and droplet diameter. Interestingly the figure also reveals the inertial quality of the liquid mode in the hysteresis loop between droplet mode and jet mode.

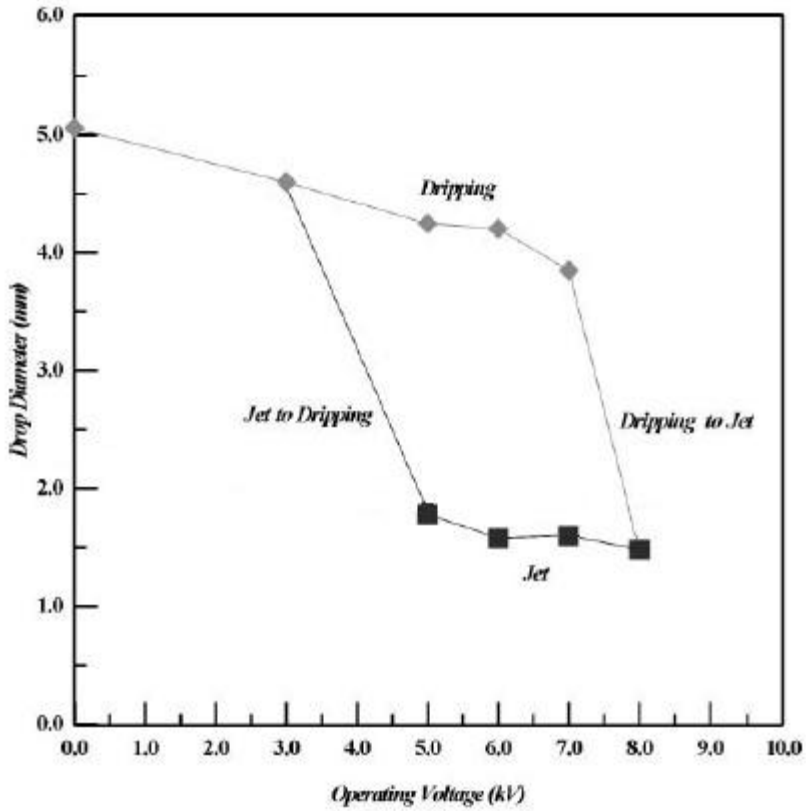


Fig. 6 Operating voltage vs 3% polyvinyl alcohol solution droplet diameter in dripping and jet modes (edited so only a flowrate of 25 mL/min displayed) [4]. The overlap in operating voltage between the two phases is a good example of the inertial properties of this process – the phases need additional energy gained or lost to instigate a transition, i.e. they tend to want to stay in the same phase (liquid or jet).

*Bending Instability*

Bending instabilities are seen in electrospinning beginning a short distance from the Taylor cone and are the fundamental reason behind the randomness of fibers deposited onto a stationary target. While initially the jet of fluid emitted from the Taylor cone travels in a straight line, likely due to the electrical and inertial force-induced longitudinal stress on the stream, the combination of repulsive electrical forces and minor deviations in linearity lead to the phenomenon known as bending instability. Because the stream of fluid emitted from a Taylor cone can be assumed to have the same charge along the axis of flight the charged stream instigates repulsive forces on

neighboring segments, magnified by turbulent deviations from linearity. This manifests itself as a random, continuous system of expansion in a general direction towards the (grounded) electrospinning target. During the expansion due to bending instabilities, the stream simultaneously loses solvent due to evaporation and stretches, producing fibers of decreasing diameter until they are deposited onto the target. Figures 7 and 8 reveal the evolution of electrical bending instability in an electrospun stream of polyethylene oxide dissolved in water and ethanol.

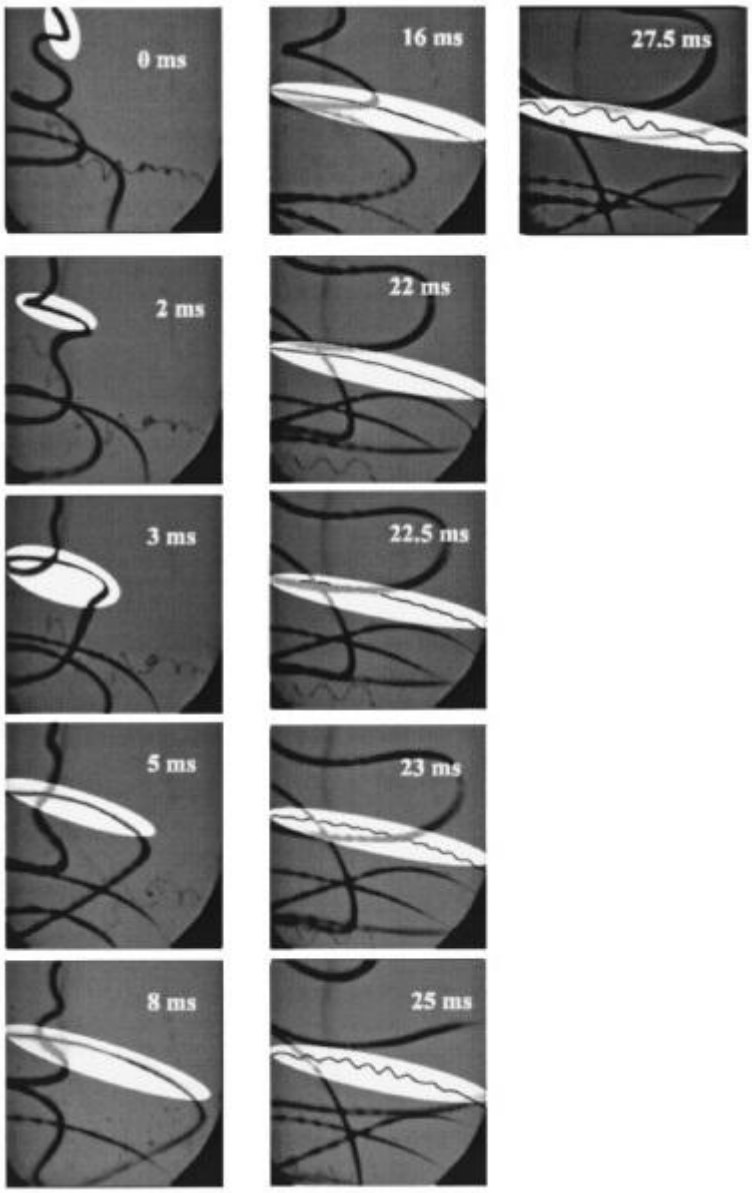


Fig. 7  Evolution of electrical bending instabilities - 0.25 ms exposure time [3].

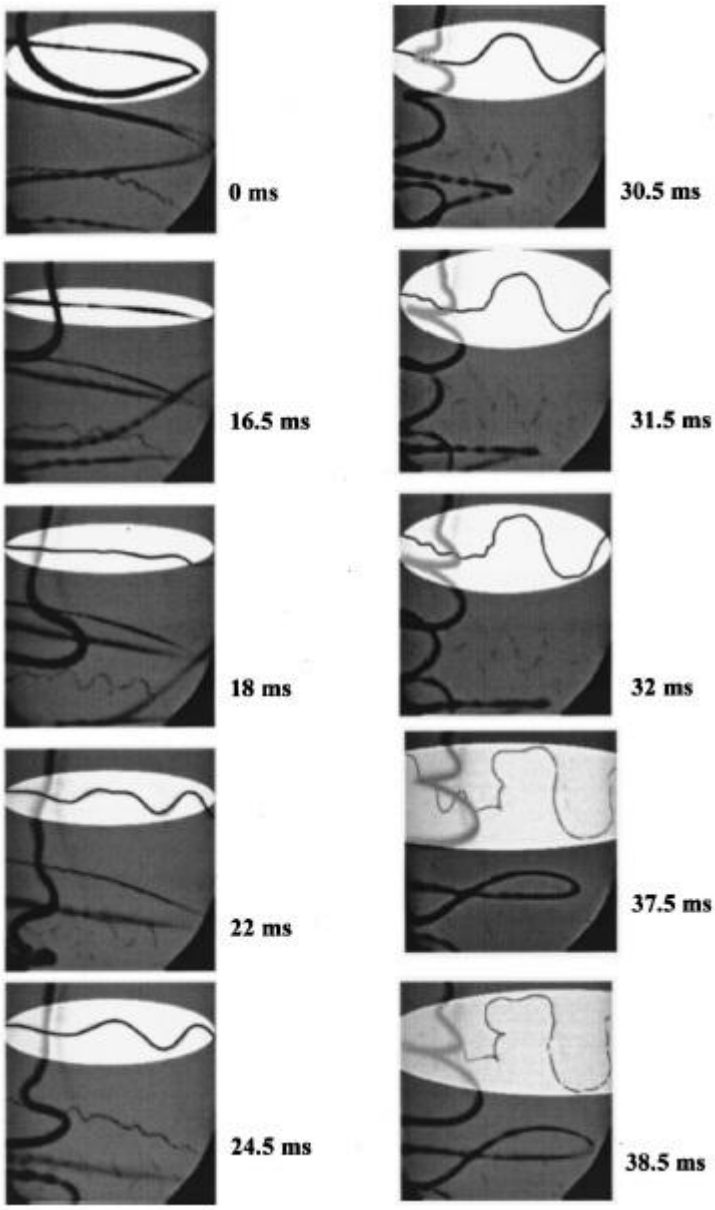


Fig. 8 Evolution of secondary and tertiary electrical bending instabilities - 0.25 ms exposure time [3].

*Fiber Solidification (Solvent Evaporation)*

Fiber solidification is based on the rate of solvent evaporation and represents a critical step in the process of electrospinning. The charged electrospinning stream exits the capillary tube as a combination of solute (typically a polymer) and solvent. The

evaporation of the solvent is based on the inherent volatility of the solvent and Fick's law of mass diffusion [2] which states that the rate of evaporation (diffusion of solvent away from the stream) is directly proportional to the surface area available for mass transfer and the gradient of mass (of the solvent) between the stream and the atmosphere. This principle is experimentally validated by Xiang-Fa, et. al. in Figure 9 where the plot of evaporation time versus initial jet radius increases exponentially as the ratio of surface area available for evaporation to volume decreases exponentially (Figure 10). Essentially, as a stream of charged fluid increases in diameter it experiences an exponential decrease in the percentage of volume available for evaporation, leading to an exponential increase in required evaporation time with linear increases in stream diameter.

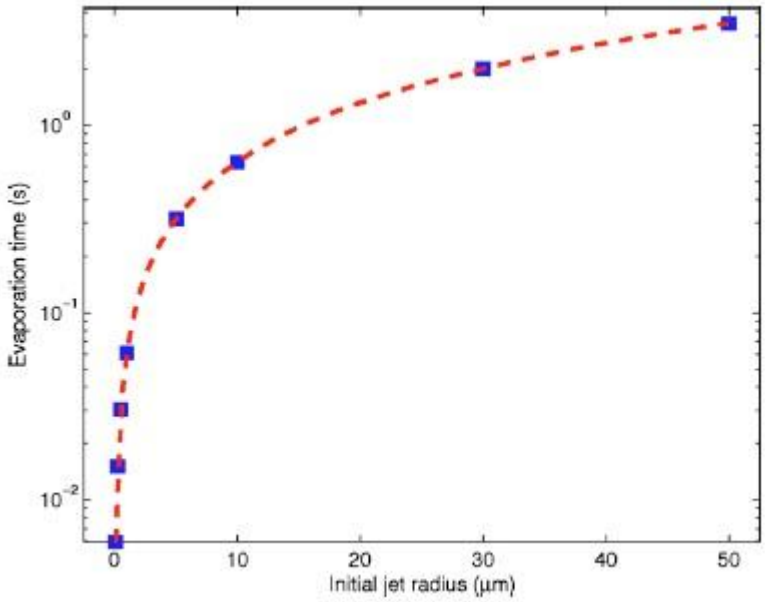


Fig. 9 Variations in jet drying time vs initial jet radius [2].

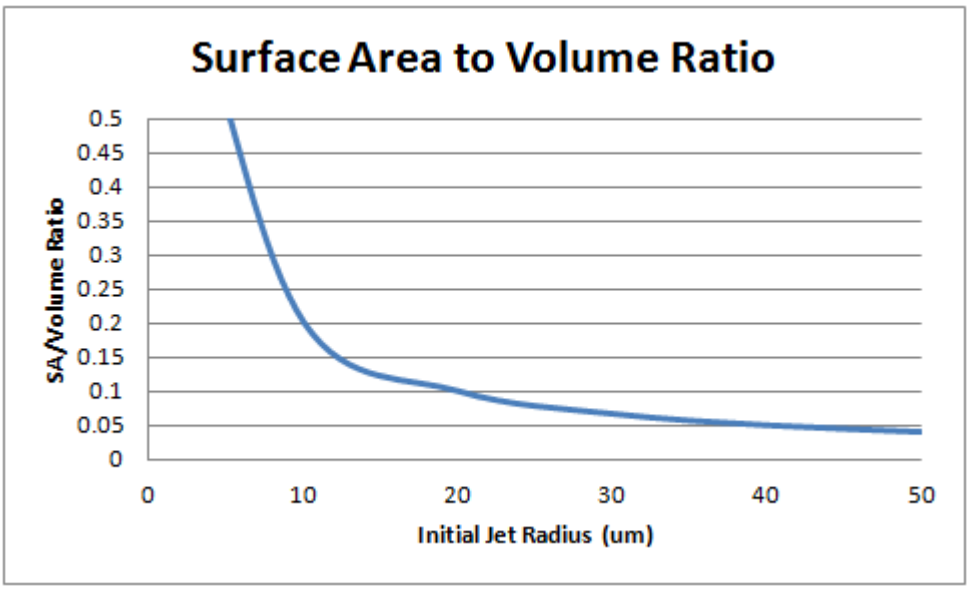


Fig. 10 Surface area (area available for diffusion) to volume ratio for an electrospinning stream.

Additional complexity is added to the system due to the bending instability phenomenon associated with electrospinning. The continuous stretching and whipping motion associated with the bending instability acts to increase the rate of evaporation through the following two mechanisms: decreasing the stream diameter and maximizing the local solvent gradient. Bending instabilities instigate elongation of the electrospinning fluid stream, decreasing the diameter and increasing the rate of evaporation (Figures 9, 10). Additionally the whipping motion associated with bending instabilities instigates evaporation rate increases analogous to the heat dissipation increases in convection vs conduction heat transfer. By continuously “whipping” the stream the instantaneous local solvent differential is held at maximal levels, similar to convection heat transfer (as opposed to a theoretical linear stream with no bending instabilities which would approximate conduction heat transfer by slowly saturating and degrading the local solvent differential). Giller, et. al. experimented with electrospinning

in environments consisting of increasing atmospheric solvent content. Figure 11 clearly shows that an inadequate atmospheric solvent differential retards solvent evaporation and hampers individual fiber formation.

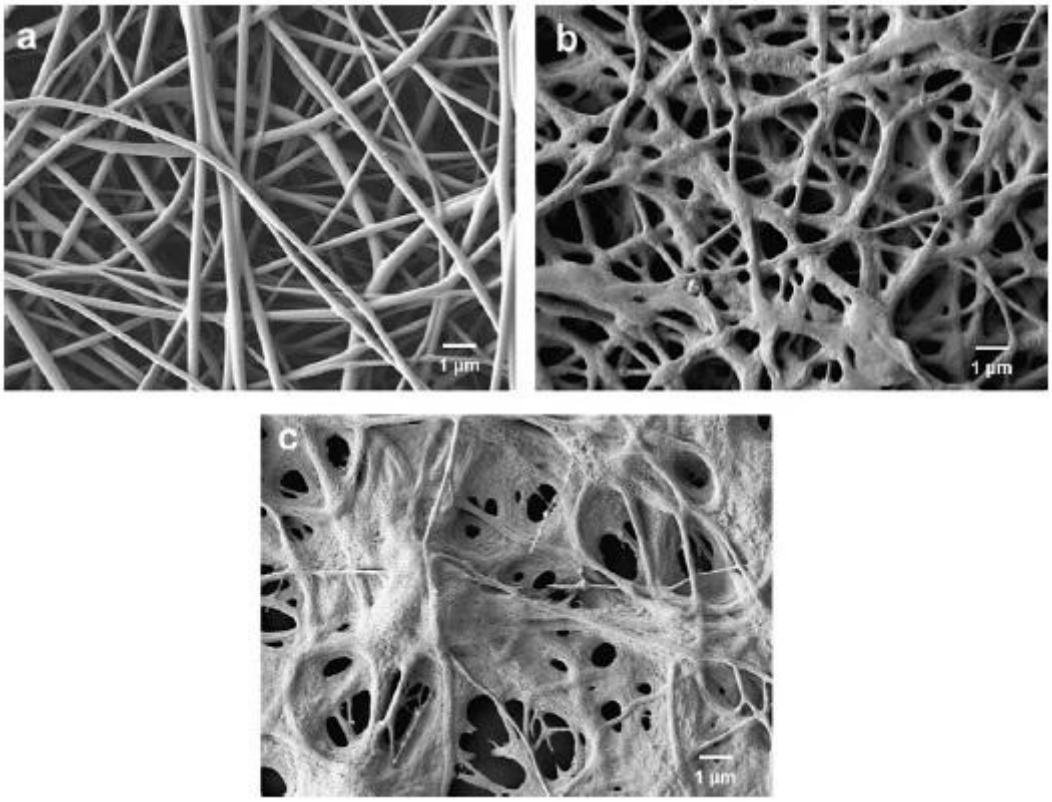


Fig. 11 SEM Images of Nylon 6 electrospun in atmospheric HFIP concentrations of a) 0 $g/m^3$ b) 106 $g/m^3$ and c) 213 $g/m^3$ [5]. Note that as the concentration of HFIP in the spinning atmosphere the resulting scaffold becomes increasingly "wet" upon deposition.

Additionally, Giller, et. al. further emphasized the innate intricacy of the electrospinning process through the analysis of fiber crystallinity [5]. In their study, they determined that a balance must exist between the rate of crystallization and solvent evaporation. Solvent evaporation essentially "locks" the crystal structure in place. If evaporation/crystallization dyssynchrony exists the crystallization process could be

incomplete at the time of fiber formation, leading to obvious inconsistencies in fiber structure.

*Fiber Collection*

The last fundamental aspect of electrospinning is target dynamics. The most important aspect of the target is its electrical potential. Typically grounded or negatively charged, the target must provide adequate electrostatic attractive forces in order to efficiently collect the charged fibers as they are spun. If the target is subjected to the same potential as the electrospun fiber there will be no attractive forces to instigate fiber accumulation and the target will have a very poor deposition efficiency.

Electrospinning in its most simple form can be accomplished by simply letting the fibers accumulate onto a grounded static target or a target placed in front of a grounded element. In this example, the electrospinning process will yield a mat of randomly oriented fibers due to the bending instabilities characteristic of charged fibers.

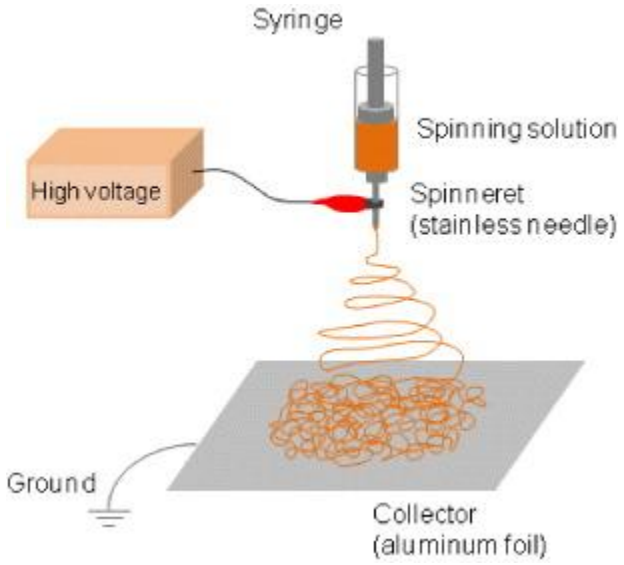


Fig. 12 Producing randomly aligned scaffolds by electrospinning onto a stationary target.

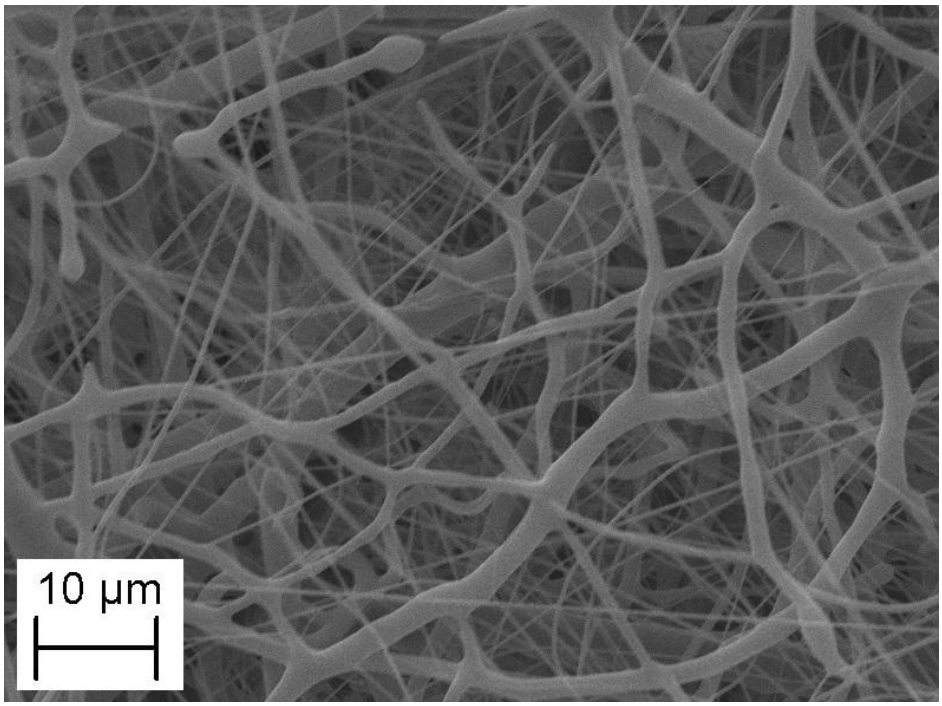


Fig. 13 SEM image of a randomly aligned electrospun scaffold (PCL 200 mg/mL, 1500x).

Fiber alignment can be achieved with many electrospinning target architectures, the two most common are high-speed rotating drums (Figure 15, 16), and the two pole air gap system developed by Jha, et. al. (Figure 14) [6].

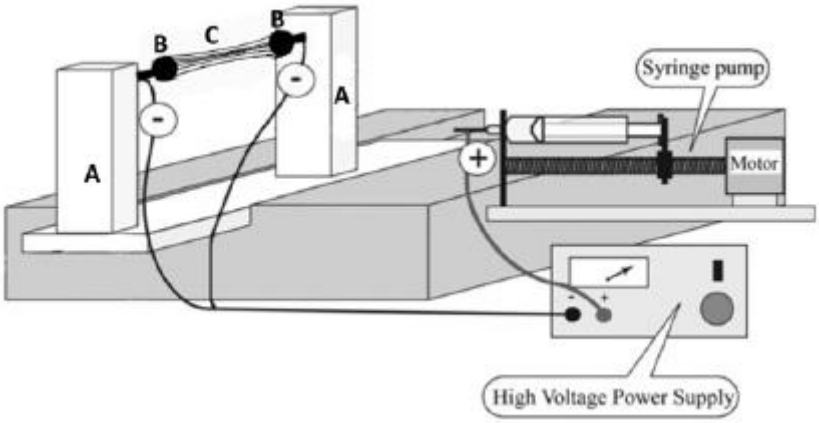

Fig. 14 Two pole air gap electrospinning apparatus with a) piers separated by a set distance b) “bullet” targets. c) Fibers form in between the targets in a highly-aligned manner [6].

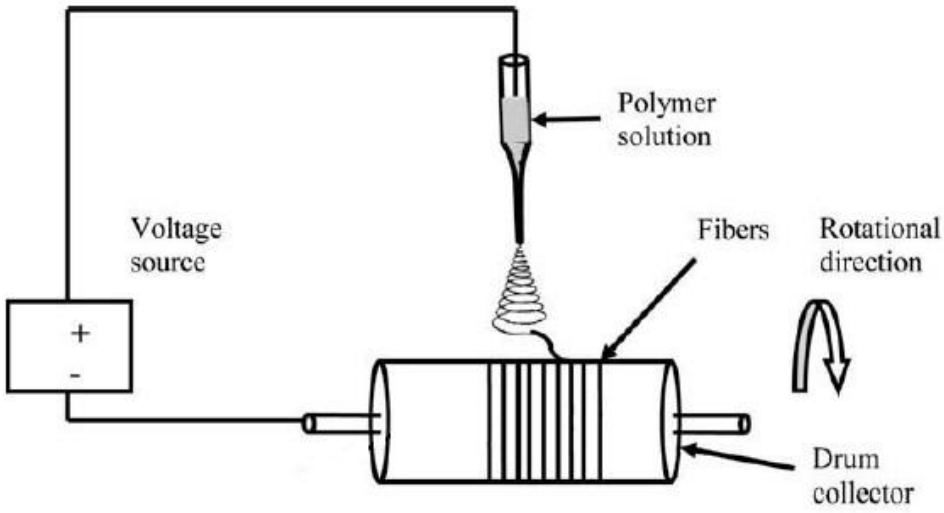


Fig. 15 Rotating drum electrospinning target [7].

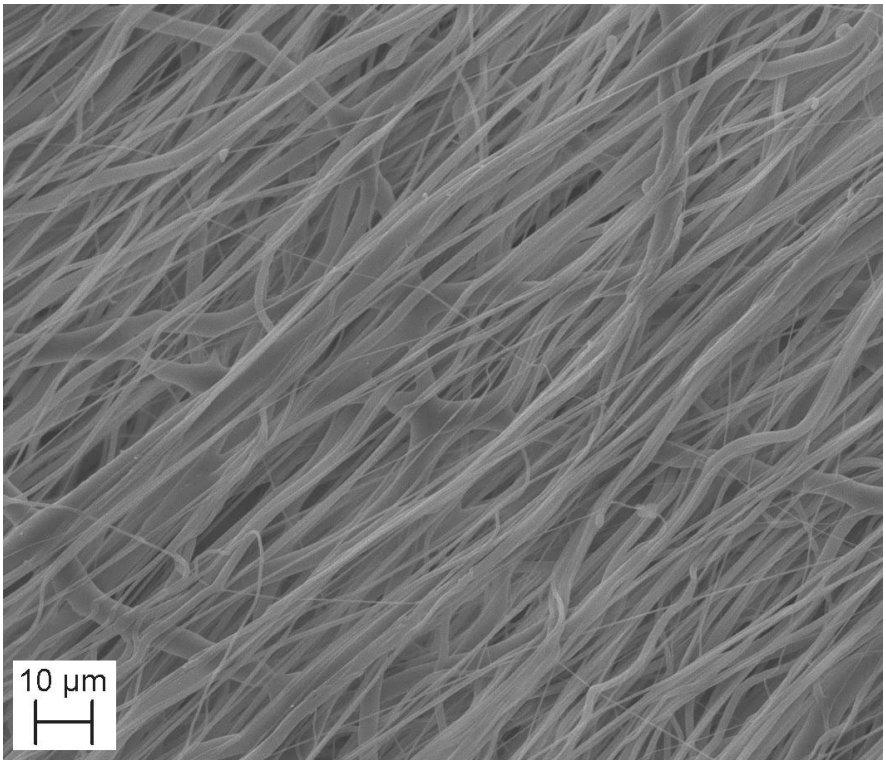


Fig. 16 SEM of aligned electrospun scaffold fabricated on a rotating drum target (PCL 200 mg/mL, 1000x).

### 1.3 Introduction to Integrated Fiber Electrospinning

The development of the integrated fiber electrospinning technique was purely need-based. Our research required the manufacturing of two types of electrospun scaffold; a highly aligned electrospun scaffold for use in long-gap nerve regeneration and an alternatingly layered electrospun mat for use as an emergency bandage. In hypothesizing future generation nerve guides, we thought to incorporate multiple levels of chemotaxic growth factors alternating between neurogenic and vasculogenic agents to simultaneously promote axon regeneration and the necessary vascular support structure. Additionally, we were manufacturing the layered bandage scaffold as a laminated structure, i.e. electrospraying a layer of structural fibers followed by the application of clotting agents and another electrospun fibrous layer until the scaffold was of the appropriate thickness. Both of these scaffolds, despite targeting very different tissues, require the same basic structural components, that is, multiple layers somehow integrated together in order to form a unified structure possessing the ability to simultaneously introduce several different types of regenerative agents. Laminating the layers was a feasible approach, however, we knew that it introduced the possibility of delamination failure because of inadequate mechanical connection between the separate layers. Our desire for a better approach brought us back to the design board and eventually to an electrospinning technique that seamlessly transitions between fibrous layers. This technique, which we labeled “Integrated Fiber Electrospinning” is the basis of this study and will be explained in much greater detail in the following sections.

### 1.4 - General Thesis Outline

The general order of this paper should be as follows:

- In depth description of current electrospinning techniques and the characteristics of scaffolds it produces.
- Introduction and explanation of our novel integrated fiber electrospinning technique.
- Materials and Methods detailing the experiments performed to compare and contrast the two electrospinning techniques.
- Results of our experiments - tensile testing, burst testing, and examining the characteristics of failure.
- Discussion of the results to determine if there are differences between the two techniques and, if so, what they are and what they could mean to tissue engineering.
- Discussion of future work and other ideas regarding electrospinning and tissue engineering.

# Chapter 2

# Materials and Methods

## 2.1 The Integrated Fiber Electrospinning Procedure

Constructing the syringe used in the integrated fiber electrospinning technique involves a series of precise steps. At the most basic level the integrated fiber electrospinning technique exploits the concept of a concentration gradient. Much like the production a electrophoresis gradient gel, gradient spinning is achieved by selectively mixing different concentrations of a given polymer, or a polymer of composed of different molecular weights, or different identities (synthetic, natural or blends of materials), and/or even polymers suspended in different solvents during the electrospinning process. Any number of combinations of materials may be blended into a continuous gradient (i.e. two, three, or more etc different materials as described). In the fabrication of a gradient gel, different concentrations of polyacrylamide are mixed at varying rates to produce a gel composed of different concentrations of polymerized acrylamide. The resulting gel has a continuously variable concentration of gel as determined by the rate of mixing. In this study this concept was exploited in the electrospinning process. Fiber size is controlled by varying the concentration of a polymer and, by carefully engineering the gradient formation, fiber size can be controlled during electrospinning. Fundamental to this process is the manufacture of

the mixing device. This was achieved by placing a mixing port between two different reservoirs within a single syringe (or other suitable reservoir). By varying the size of the port the extent of mixing that occurs during the electrospinning process, at the interface of the reservoirs, can be controlled. Mixing of the polymers occurs at the juncture of the two reservoirs rather than at the needle tip. Construction of this mixing device can be achieved, for example, by:

Step 1 - Remove the plunger from a 3 mL BD syringe, attach a blunted 18 gauge needle tip (capillary tube), and wrap the blunted tip with parafilm to prevent fluid escape.

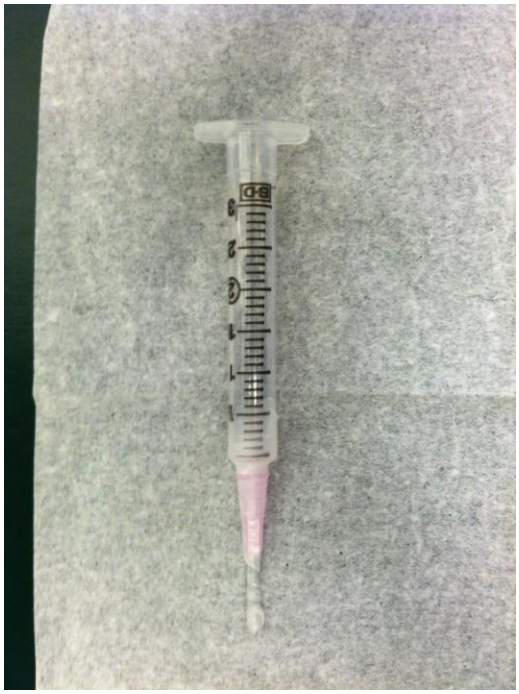

Fig. 17 Integrated Fiber Electrospinning - Syringe Manufacturing Procedure Step 1.

Step 2 - Pierce the rubber plunger tip from a 3 mL BD syringe with an 18 gauge needle.

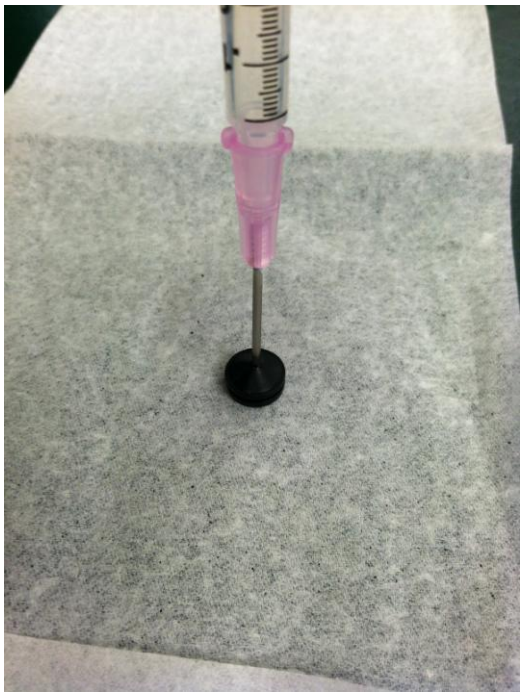

Fig. 18  Integrated Fiber Electrospinning - Syringe Manufacturing Procedure Step 2.

Step 3 - Obtained a small tubular section from an 18 gauge needle tip (note: care must be taken not to pinch the ends of this section so as not to restrict fluid flow).

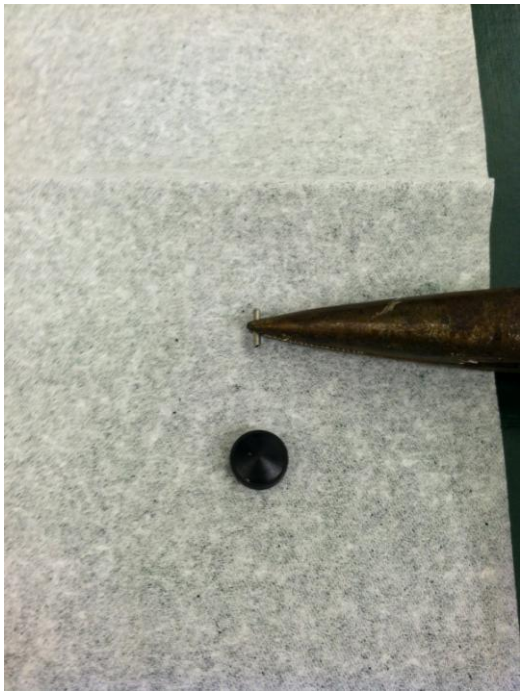

Fig. 19  Integrated Fiber Electrospinning - Syringe Manufacturing Procedure Step 3.

Step 4 - Insert the tubular needle section into the perforated rubber plunger tip. This completes the manufacturing of the semi-permeable membrane that will separate the electrospinning solutions.

Fig. 20 Integrated Fiber Electrospinning - Syringe Manufacturing Procedure Step 4.

Step 5 - From the void created by removing the plunger, fill the integrated electrospinning syringe with the first electrospinning fluid and place the intermediate disk into the syringe, containing the first fluid to the needle end of the syringe. In this study 1.5 mL polycaprolactone (PCL) at 100 mg/mL was used as the first electrospinning fluid.

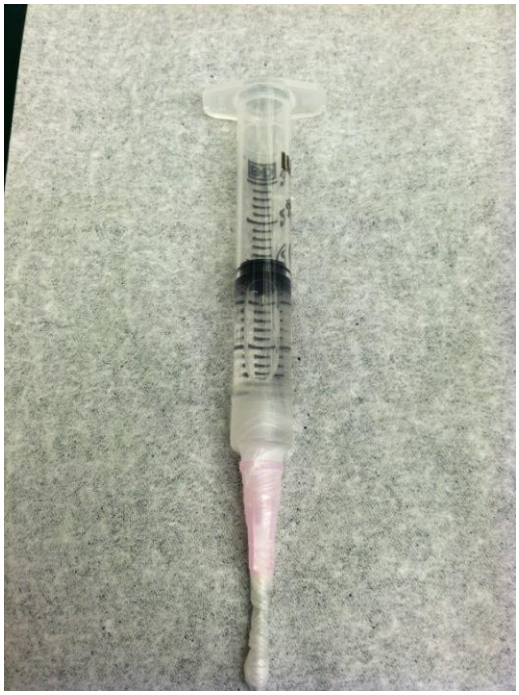

Fig. 21 Integrated Fiber Electrospinning - Syringe Manufacturing Procedure Step 5.

Step 6 - Remove the residual air in the first compartment by puncturing the syringe wall with a small gauge needle at fluid level. Once the wall is punctured the intermediate disk can be further depressed to force the residual air out. Care must be taken to remove only the air and no electrospinning fluid. Once the air is removed seal the hole with parafilm.

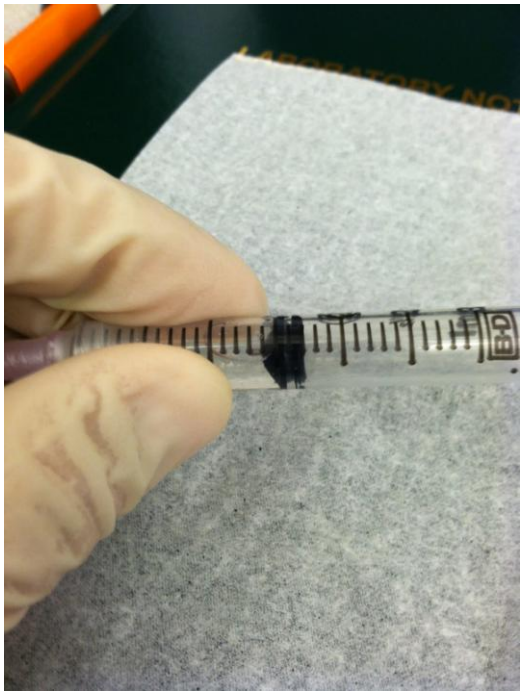

Fig. 22 Integrated Fiber Electrospinning - Syringe Manufacturing Procedure Step 6 (note the air bubble).

Step 7 - From the void created by removing the plunger, fill the integrated electrospinning syringe with the second electrospinning solution.  If more than two solutions are desired simply insert additional intermediate disks behind each fluid layer.

Fig. 23  Integrated Fiber Electrospinning - Syringe Manufacturing Procedure Step 7.

Step 8 - Insert a non-perforated rubber plunger tip behind the last electrospinning fluid to close the system. We found it necessary to temporarily perforate the plunger with a small needle during this step.

Fig. 24 Integrated Fiber Electrospinning - Syringe Manufacturing Procedure Step 8.

Once the final plunger is in place the syringe is ready for electrospinning. While the basic electrospinning procedure doesn't change in integrated fiber electrospinning, we were typically forced to vary the applied electrical potential in order to maintain a stable Taylor cone as the electrospinning fluid transitioned. By design this process renders the fluid and conductive properties of the electrospinning solution dynamic in nature so the requirement of varying the electrical potential to optimize spinning was not a surprise.

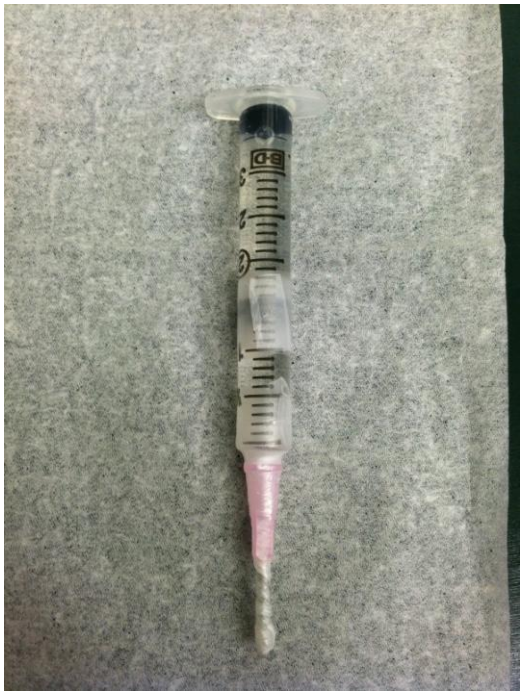

Fig. 25  Integrated Fiber Electrospinning - Syringe Manufacturing Procedure - completed syringe

**2.2 Limited Transition Integrated Electrospinning Technique**

When we envisioned the integrated fiber electrospinning technique we imagined the intermediate plunger traveling in synchrony with the permanent plunger.  Despite reducing the intermediate channel to our smallest needle section (26-gauge, results not shown) the intermediate plunger continually failed to travel down the syringe body until the permanent plunger came into contact with it (after which it was physically pushed down the syringe).  [It should also be noted that we attempted to simply perforate the intermediate disk with varying needles and, while we did succeed with this method to propel the intermediate disk down the syringe body in synchrony with the permanent plunger, once it reached the end the self-sealing properties of the plunger tips became evident as it did not allow fluid to pass.]

To remedy this design problem we developed a new electrospinning technique called “Limited Transition Integrated Electrospinning.” First we removed the needle section from a 22-gauge needle and placed it into the luer-lock end of a blunted 16-gauge needle as shown in Figure 26. The 16-gauge needle section was bent to lock the 22-gauge needle tip in place.

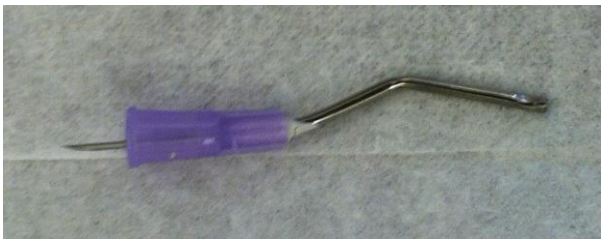

Fig. 26 A 22-gauge needle inserted into luer-lock end of 16-gauge needle.

Next we attached the customized 16-gauge needle onto a 3mL BD syringe as shown in Figure 27. By locking the 22-gauge needle section in place we created a perforating element inside the body of the syringe. With this device in place a communicating channel through the intermediate disk was no longer necessary as communication would be established when the intermediate disk reached the bottom of the syringe and was perforated by the 22-gauge needle. Once the intermediate disk becomes perforated, fluid travels through the 22-gauge needle section and out of the 16-gauge needle to be electrospun.

Fig. 27  Customized 16-gauge needle on a 3mL BD syringe.

Figure 28 shows the limited transition integrated electrospinning system in action. It's apparent in this figure that the intermediate disk is traveling down the syringe body via the fluid pressure rather than contact from the permanent plunger (note that, at the initiation of electrospinning the intermediate disk is located in the middle of the parafilm coating and has traveled down the syringe body to become visible).  Limited testing was performed on this technique as it produced a nearly laminated scaffold.

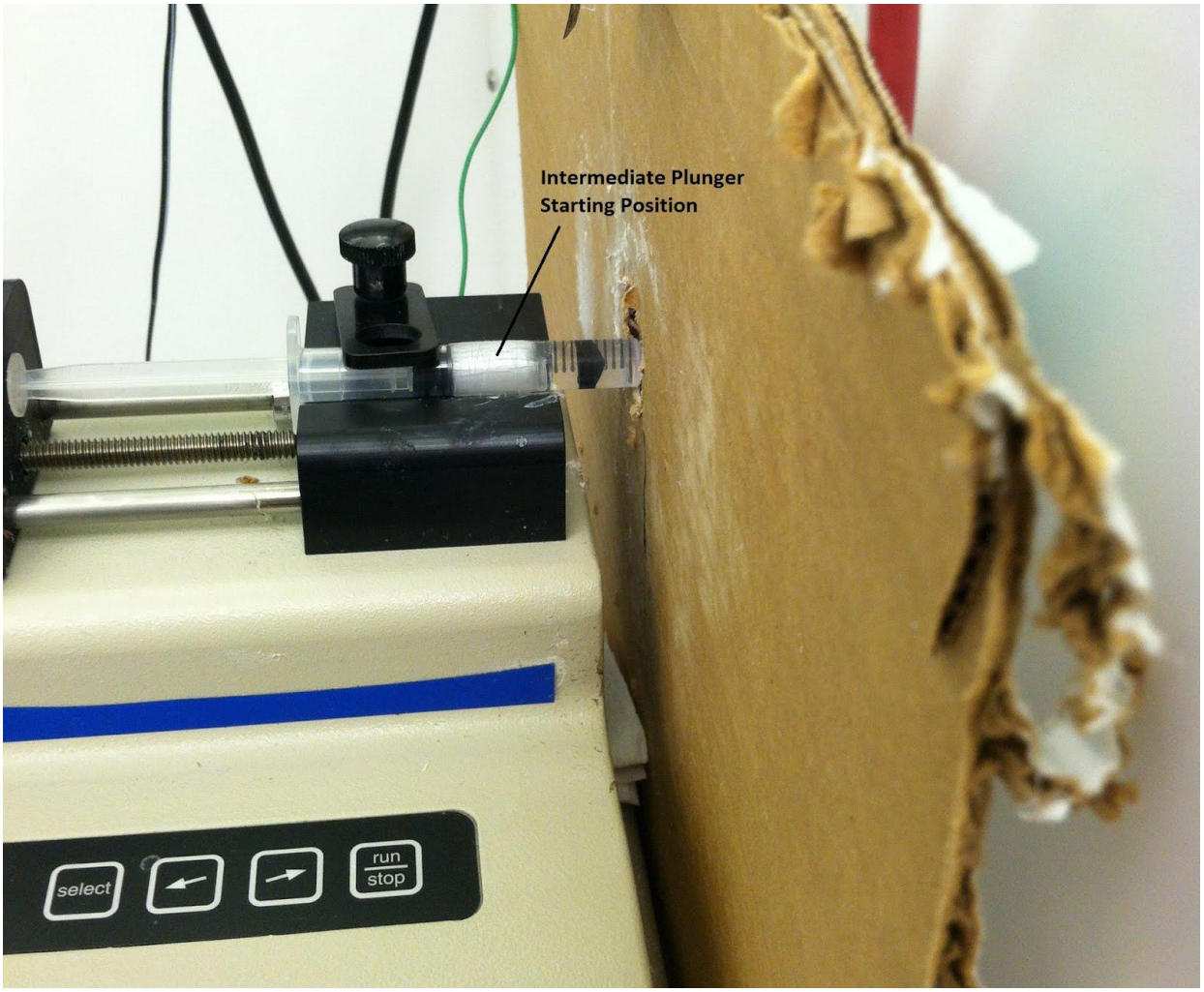


Fig. 28 The limited transition integrated electrospinning system in action.

### 2.3 Experimental Electrospinning Techniques

Electrospinning was performed in Dr. Gary Bowlin's lab utilizing a Fisher Scientific 110V, 60 Hz syringe pump to provide steady flow of electrospinning fluid at a rate of 8 mL/hour to either 3 mL or 10 mL BD plastic syringes utilizing an 18-gauge blunted needle as the capillary tube. To provide static potential and initiate electrospinning we employed a Spellman 0-30 kV DC power supply. Electrospinning took place across a fixed 20 cm gap onto a grounded cylindrical metal target with a

length of 11.75 cm and a diameter of 6.33 mm. Via a DC motor speed control (Custom Design and Fabrication) the cylindrical target was designed to both rotate and slide in order to collect an evenly-coated scaffold of varying alignment. In this study low-speed electrospinning (randomly aligned scaffolds) was performed at the “0” rotational speed setting which equated to 694 rpm. High-speed electrospinning (aligned scaffolds) was performed at the “6” rotational speed setting which equated to 7090 rpm (both of these determined with Extech Digital Stroboscope). The electrospinning compartment itself was a completely closed container with a dedicated exhaust system to remove atmospheric solvent and contaminate factors. The average temperature and humidity experienced in the lab was 72 degrees Fahrenheit and 30% humidity. In this study polycaprolactone (PCL) was the sole electrospinning polymer. Our PCL was purchased from Sigma Aldrich having a molecular weight of 65000 Daltons. To electrospin it was put into solution using the solvent 2,2,2 - Trifluoroethanol - 99.8% (TFE) which was purchased from Acros Organics.

Scaffolds produced from 100 mg/mL PCL, 200 mg/mL PCL, and gradients of PCL were used in this study. Gradients were produced after the methods described in the background section of this document using two reservoirs within a single syringe connected by either an 18-gauge or a 22-gauge port. It should be noted that the use of a port allows for additional control in the mixing process, making it more predictable and reproducible. However, gradient spinning can be achieved without such a port, and that port can be envisioned in any number of ways including varying diameters, numbers, and even substitution of the intermediate disk with meshes and semi-permeable membranes. Of note, spinning from 100 mg/mL PCL produces very small diameter

fibers. Scaffolds composed of these fibers can be quite delicate, however, by using this concentration it is possible to clearly identify changes in concentration as the gradient begins to exert effects on structure of a scaffold. In this study laminated structures represent those scaffolds that were spun in two separate and discrete layers; a layer of fibers produced from 100 mg/mL PCL and a separate layer produced from 200 mg/mL PCL.

### 2.4 Determining Instantaneous Polymer Concentration in Electrospinning

A surprising challenge in this study was determining the instantaneous concentration of PCL as it was expelled by a syringe in an electrospinning apparatus. This information is important to determine the efficacy of different electrospinning designs that eventually lead to our integrated fiber electrospinning technique. In these experiments we determined this variable simply by setting up the solutions of interest within the reservoir to be tested. The resulting syringe was then placed into a syringe pump as if it were to be electrospun. The pump was then turned on in the absence of an electric field and the expelled polymer was collected into individual weigh dishes at two-minute time intervals. All residual weight analyses were conducted using a flow rate of 8 mL/hr (the same flow rate used in actual electrospinning), fluids were dispensed from an 18 gauge blunted needle tip. This residual weight analysis proved to be an easy and accurate method for determining the efficacy of different electrospinning techniques. Additionally, by removing the electrostatic element, the tests could be easily performed without the added risks and requirements present when actually

initiating electrospinning. We (correctly) assumed that by collecting samples at set time intervals we could create a plot of polymer concentration with respect to time.

The challenge was identifying the assay method to determine the concentration of the fluid that we were collecting. After many failed assays involving serum-doped PCL ELISA's and undoped ELISA's to try to tease out photoluminescent differences in the different concentrations of PCL the humbling eureka moment came. The way to determine instantaneous polymer concentration was simply to collect the fluid at set time intervals, allow the solvent to completely evaporate off, and then weigh the residual polymer which does not evaporate. Because the flow rate is constant at 8 mL/hr the total quantity of fluid is easily ascertained and then the concentration can be extracted by the weight of the residual polymer. An easy example of this would be to collect fluid for 15 minutes at a flow rate of 8 mL/hr, to collect a total volume of 2 mL. If the residual polymer weighed 400 mg then the concentration of the polymer is simply 400 mg / 2 mL, or 200 mg/mL. Likewise if 200 mg was collected then the concentration of the polymer is 100 mg/mL.

The dry weight analysis provided us with a metric that, when paired with the corresponding fiber diameter analysis, provides clear evidence for the dynamic nature of integrated electrospinning process. The varying polymer concentration that we detected allowed for the formation of structures that had a "gradient" of fiber diameters.

### 2.5 Fiber Diameter Analysis

Fiber diameter analysis was performed in a similar fashion as the dry weight analysis, the most notable change was the addition of electrospinning. In these

experiments we collected electrospun samples at two-minute intervals to create a graph of fiber diameter versus electrospinning time. It was found that the easiest medium to capture the fibers was on a black section of paper. Paper is easy to shape to cut and fit into the electrospinning chamber and the black background makes it easy to see the fibers depositing. In order to safely collect samples at two minute intervals, during the spinning process we would de-energize the system by turning off the DC power supply, place the sample paper target over the sliding drum (note that drum rotation was not used in this experiment), and then re-energize the system to initiate electrospinning onto the sample target. It's important to note that the syringe pump was not stopped throughout this process - even though "true" electrospinning was interrupted by the de-energization of the power supply the flow out of the syringe was held constant therefore the fluid dynamics in the syringe should be identical to those used in continuous "true" electrospinning (no interruption in static potential). This method succeeded in giving us instantaneous snapshots of fiber diameters that we were able to then analyze (Figure 29).

The actual fiber analysis was performed by imaging the scaffolds at a constant magnification of 1500x utilizing the Zeiss EVO 50 Scanning Electron Microscope (SEM) courtesy of VCU microscopy. The images were captured at a minimum resolution of 1024x768 which provided more than sufficient detail to perform these tests. In an effort to eliminate bias in the analysis of fiber diameters a uniform half-grid was placed on the samples and only the fibers that crossed the designated lines were measured. Actual fiber measurement was performed using the program ImageJ which allows the user to

define a known length for a pixel range (via the scale bar on each image) and then convert manually measured distances across fibers, in pixels, to microns for analysis.

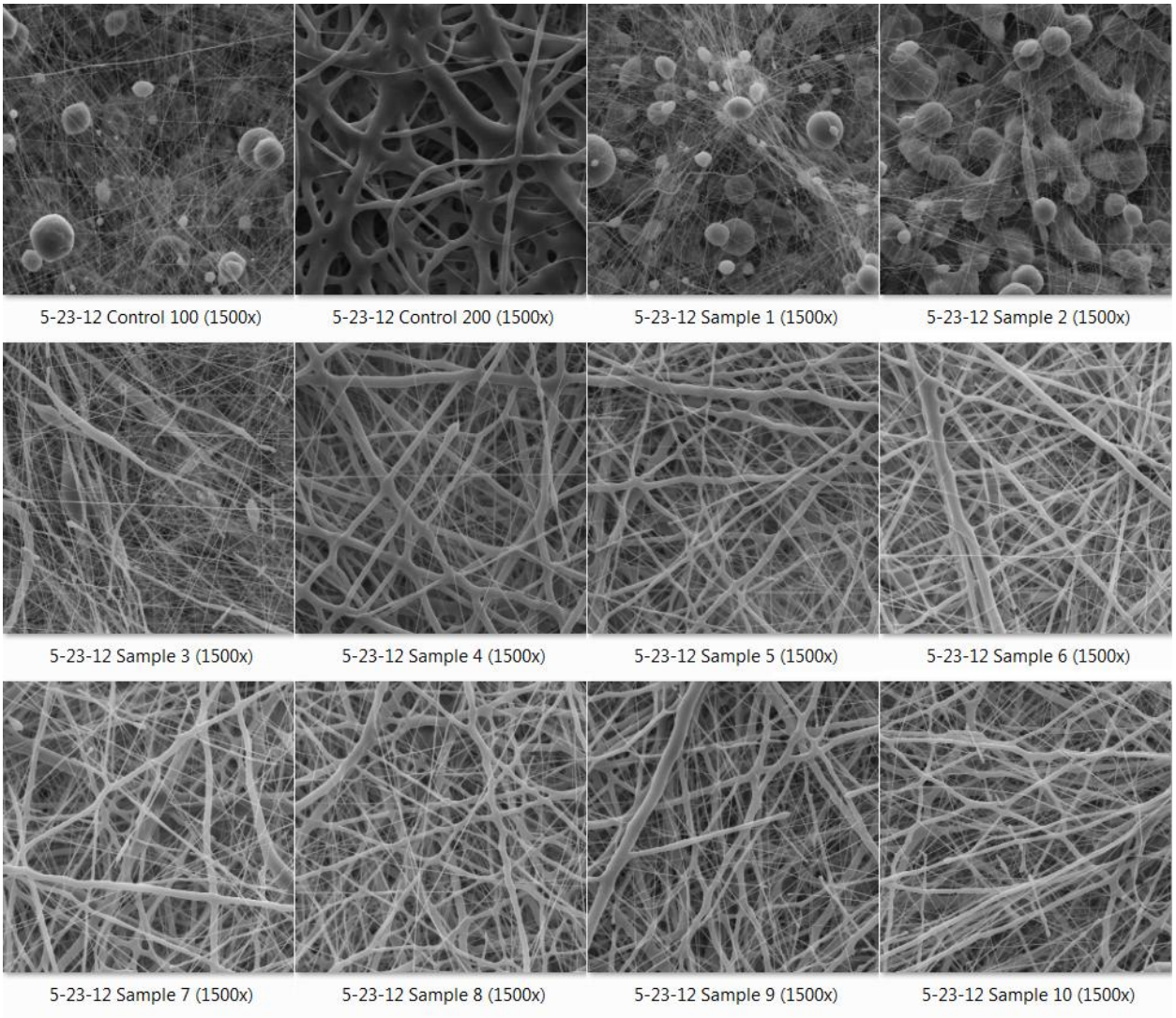


Fig. 29 Example of electrospun fibers captured at two-minute intervals. The average fiber diameter for each sample was recorded and plotted vs. time.

### 2.6 Tensile Testing

Scaffold mechanical properties were characterized by conventional tensile testing using a MTS Bionix Tensile Test System with a 100N load cell. Scaffolds were spun using a total volume of 3.5 mL whenever possible, the major exception being 100

mg/mL control scaffolds as a volume of 3.5 mL did not yield a testable construct. The minimum volume for 100 mg/mL control scaffolds was approximately 10 mL. Because tensile testing controls for scaffold thickness the solution volume was not of great concern as long as the resulting scaffold came out to an appreciable and measurable thickness. Once the scaffolds had been spun the entire drum was soaked in ethanol for five minutes to loosen the scaffold from the drum. After soaking we gently slid the scaffold off of the drum, however, if it resisted removal we simply repeated the soaking process. Once the scaffold had been successfully removed from the drum it was placed overnight in a Fisher Scientific drying chamber to remove any excess moisture and alcohol. Next the scaffolds were cut lengthwise and unrolled. Once flattened we isolated tensile testing "dog-bone" samples using an ODC Tooling and Molding Sharp-Edge Die (6.2 x 18.6 mm), this was done both in the direction of rotation ("parallel") and 90 degrees from the direction of rotation ("perpendicular"). This process created a sample with wider sections at the ends for gripping and a controlled thinner section in the middle. The middle section is known as the "test section" and is critical in tensile testing. Sample thickness, in inches, was recorded with Mitutoyo Absolute calipers and input to the tensile test computer program TestWorks4. The scaffolds were then individually placed into the tensile grips and secured. Once the samples had been secured the program was initiated at which time the samples were subjected to a rate of strain of 10 mm/min until scaffold failure. Scaffold failure is defined as when the scaffold physically breaks apart, it must do so in the test section where the dimensions of the scaffold are controlled for and placed into the stress equations. Any failure outside of the test section was not recorded. The load cell on the tensile test apparatus

measured the force resisted by the scaffold during testing and graphed it accordingly. Maximum stress and strain levels were recorded for analysis. After testing the samples were saved for subsequent SEM analysis of microstructural changes associated with scaffold failure (e.g. delamination, fiber alignment in the direction of strain, etc).

### 2.7 Burst Testing

Our second measure of scaffold mechanical properties was burst testing. Just as in tensile testing, scaffolds were spun using a total volume of 3.5 mL whenever possible, the major exception being 100 mg/mL control scaffolds which required a larger volume to yield testable scaffolds. While the burst test itself does not control for scaffold thickness, we did take it into consideration in our stress calculations so, as with tensile testing, variations in scaffold thickness were not cause for great concern (given the dynamic properties of electrospinning, especially with our novel technique, minor variations in thickness are to be expected). Once the scaffolds had been spun the entire drum was soaked in ethanol for five minutes to loosen the scaffold from the drum, after which we gently slid the scaffold off of the drum, however, if it resisted removal we simply repeated the soaking process. Notably difficult to remove were the aligned scaffolds and the 100 mg/mL scaffolds. Difficulties in removing aligned scaffolds were two-fold: first they seemed to possess a compressive grip on the drums but also the alignment was 90 degrees from the direction of removal so extra care had to be given due to the fact that the scaffolds are inherently weaker in that direction (there are very few fibers aligned in that direction to resist load so they tend to simply pull apart). Once

the scaffold had been successfully removed from the drum it was placed overnight in a Fisher Scientific drying chamber to remove any excess moisture and alcohol.

Burst testing involves introducing radial force onto the scaffold until failure. To achieve this we first had to isolate a two inch-long section scaffold and ensure that both ends of the tube were open and that the scaffold had no obvious defects along its structure. Next we fixed a two inch section of balloon to the air source via suture (all sutures used were 3-0 silk braided surgical sutures). Once one end of the balloon was fixed in place we slid the scaffold over the balloon section and sutured it to the supply section. Next we pulled the open end of the balloon through the scaffold and secured it to the other end of the apparatus, making sure to place a suture to close the system. Finally we sutured the open end of the scaffold to close the entire system. At this point the scaffold was ready for burst testing (Figure 30).

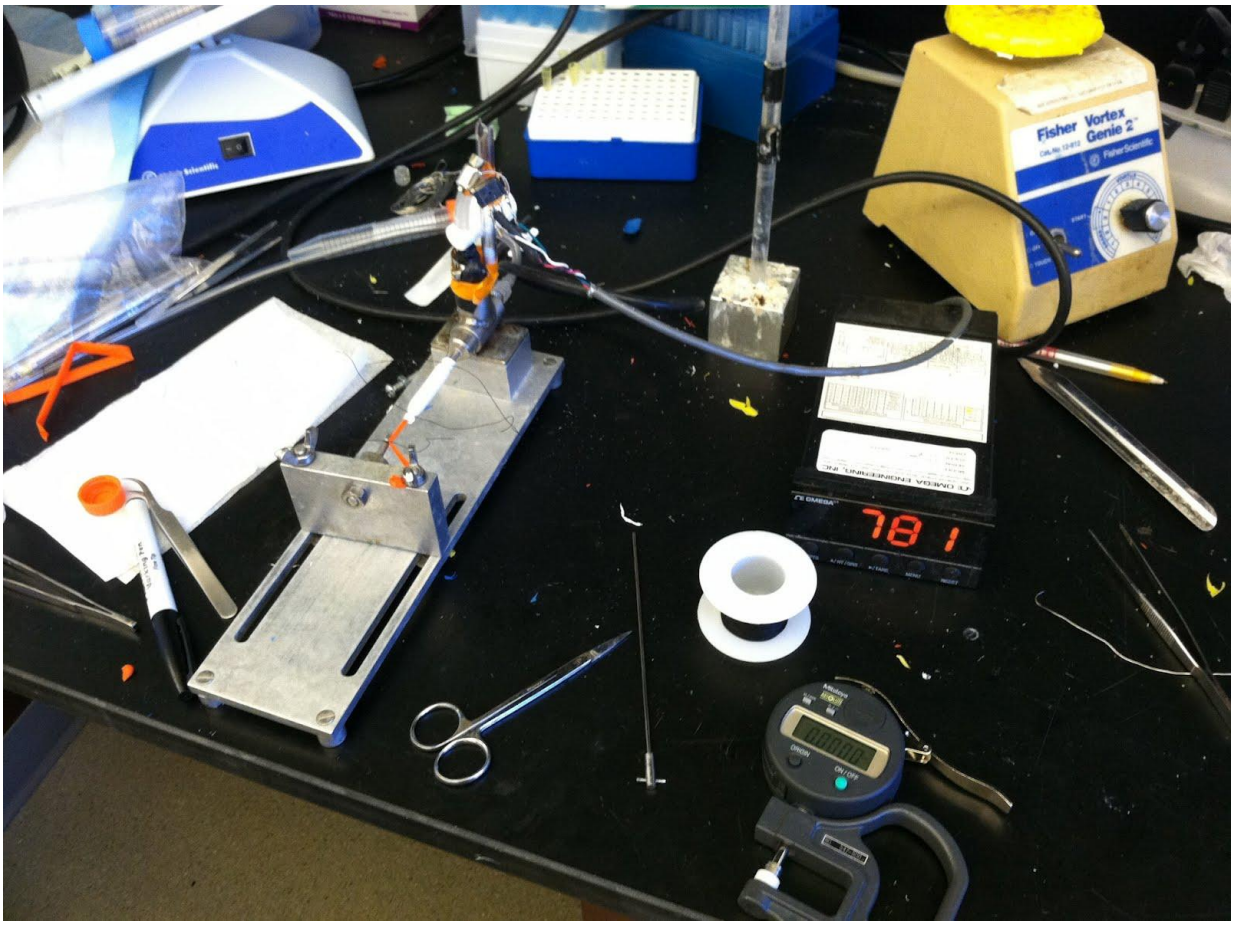


Fig. 30  Burst Testing Setup.

The testing involved manually increasing the applied radial pressure (Figure 31), as measured by an Omega Engineering Indicator, at a rate of 5 mmHg/s until the scaffold failed.  Failure is defined as scaffold fracture and, in all samples, occurred in a very catastrophic manner.  The pressure at failure was recorded for all samples as the "burst pressure."  It must be noted that any failure near the sutures was not recorded as they could have been due to extraneous variables.  Additionally, before testing the thickness of each samples was measured and recorded for input into the Hoop Stress equation (Equation 1).  It should be noted that the hoop stress equation used in this study had two major assumptions, one of which was completely satisfied throughout all

experiments. The thin wall assumption required for this equation is satisfied because the wall thicknesses of our scaffolds were consistently less than 1/10 the radius of the whole scaffold. The last assumption is that of scaffold isotropy. In our random scaffolds, despite hints of alignment seen in strain testing (Figure 37), isotropy can be quite accurately assumed. In aligned scaffolds, however, isotropy surely does not exist. Because of this we acknowledge that, in aligned scaffolds, the hoop stress data recorded is only comparative to the other aligned scaffolds and should not be taken as the true hoop stress of the material. Despite this, comparatively viewing the hoop stress results for aligned scaffolds did bring to light the valid differences in burst strength.

$$\sigma_\theta = \frac{Pr}{t} \text{ (for a cylinder)}$$

$$\sigma_\theta = \frac{Pr}{2t} \text{ (for a sphere)}$$

where

- $P$ is the internal pressure
- $t$ is the wall thickness
- $r$ is the inside radius of the cylinder.
- $\sigma_\theta$ is the hoop stress.

Eq. 1 Hoop Stress [12]

Fig. 31  Manually increasing the applied radial pressure to scaffold.

**2.8 Statistics**

Unless stated otherwise, all statistical analysis was based on a Kruskal-Wallis one way analysis of variance on ranks and a Holm-Sidak pair-wise multiple comparison procedure (alpha = 0.05).

# Chapter 3

# Results

## 3.1 Analysis of the Integrated Fiber Electrospinning Mixing Characteristics and Subsequent Fiber Formation

In this section we evaluated our novel integrated fiber electrospinning technique. Through several assays we determined the polymer mixing characteristics of our technique and the subsequent fiber dynamics that formed through electrospinning with a changing polymer concentration. With tensile and burst testing we then explored the mechanical consequences of constructing an electrospun scaffold with our technique and compared it to conventional electrospinning.

### 3.1.1 18 Gauge Intermediate Section

The first experiment involved analysis of the integrated fiber electrospinning system in a horizontal setup, that is, the syringe was on a level plane with its target. Both the dry weight analysis and the fiber diameter analysis show gradual mixing tendencies when using the intermediate disk with a perforating 18 gauge needle section (Figures 32 and 33). These graphs also allude to the fact that, while the concentration does reach the maximal level, it is certainly not maintained for a substantial length of time. Rather, there is a noticeable tail off in the last several minutes of spinning. We

have conducted tests using a vertical integrated fiber electrospinning setup in addition to the horizontal one discussed in this study (data not shown). The mixing properties, not surprisingly, can be further modulated by the position of the polymer source with respect to the target.

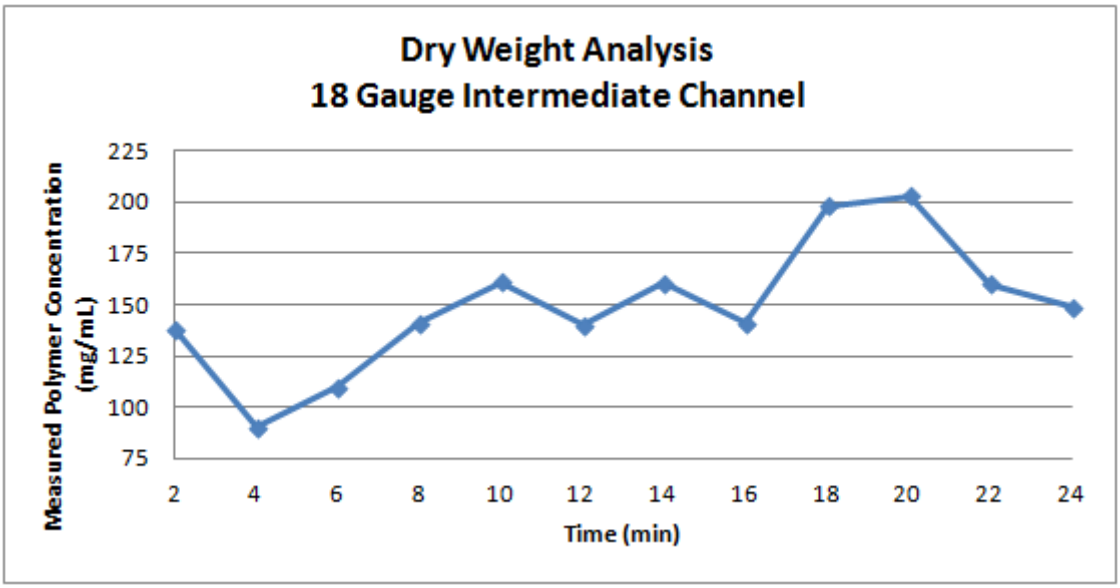


Fig. 32 PCL dry weight assay (18-gauge needle as intermediate channel).

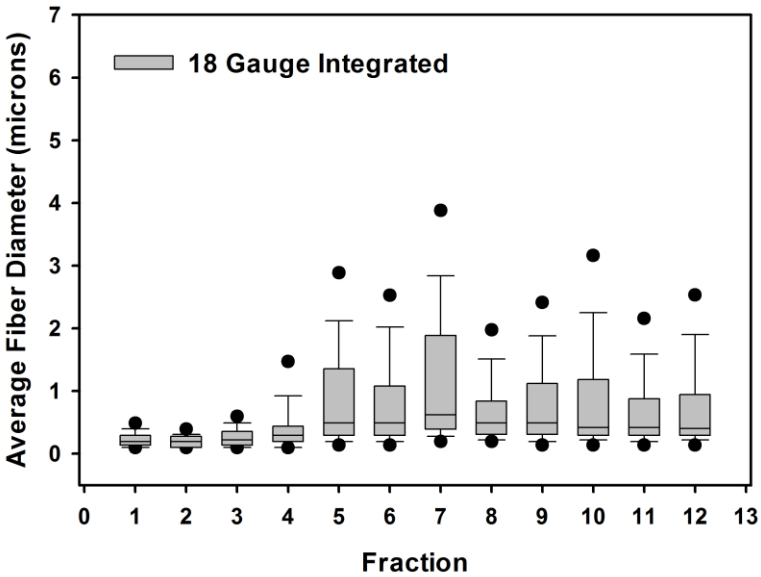


Fig. 33 Average fiber diameter analysis (18-gauge needle as intermediate channel).

### 3.1.2 22 Gauge Intermediate Section

The second experiment again utilized the horizontal electrospinning setup but reduced the diameter of the channel through the intermediate disk from 18 gauge to 22 gauge. Because the flow rate is held constant it was hypothesized that the reduction in communicating area would either 1) increase the fluid velocity through the intermediate channel if the intermediate plunger remained stationary or 2) the reduction in communicating area would impart enough force on the body of the intermediate plunger to cause it to move synchronously as the main plunger was depressed, limiting mixing. Every syringe that was tested with a 22 gauge intermediate channel behaved the same with no intermediate disk movement until the true plunger came in contact with it. The results from the dry weight analysis indicate a smooth transition in PCL concentration starting out at 100 mg/mL, beginning to transition at around minute 6, and then leveling off around minute 12 at a concentration of 150 mg/mL. The average fiber analysis echoed the dry weight results displaying a smooth transition beginning from the 100 mg/mL control average diameter of around 0.2 um, starting to transition around minute 6, and finally leveling off, though not quite as smoothly as the dry weight analysis, at around minute 12 at an average fiber diameter of 0.75 um.

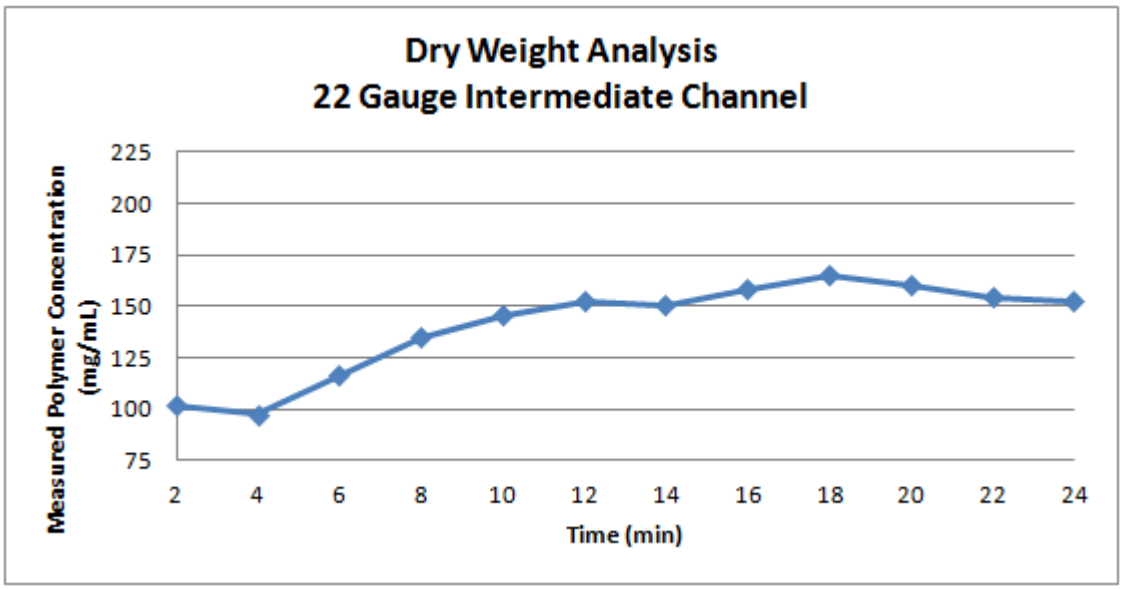


Fig. 34 PCL dry weight assay (22-gauge needle as intermediate channel).

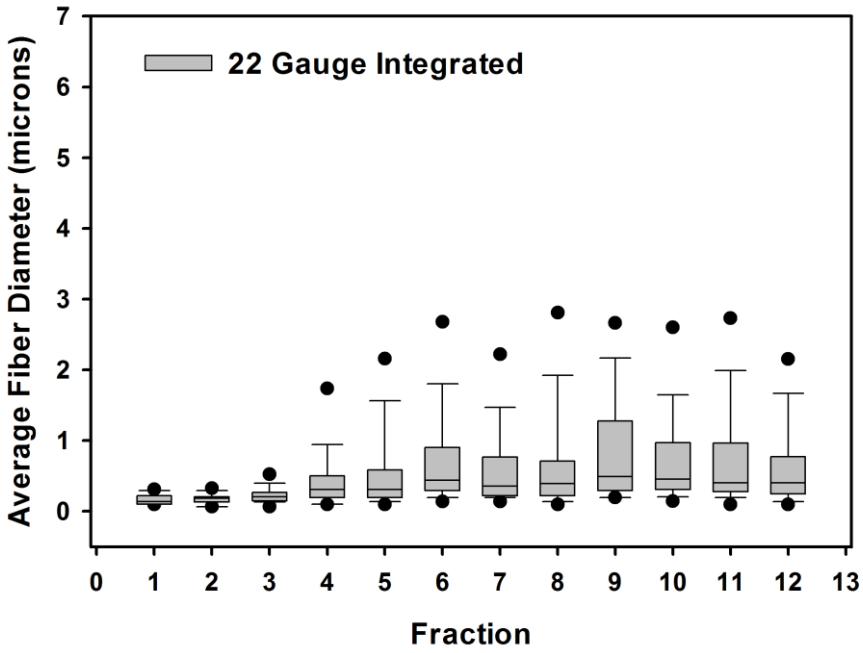


Fig. 35 Average fiber diameter analysis (22-gauge needle as intermediate channel) .

### *3.2 Tensile Testing*

In tensile testing the lowest stress values were recorded for the 100 mg/mL control groups, followed by laminated scaffolds, integrated (22G port), integrated (18G

port), and finally the strongest were the 200 mg/mL controls. The integrated scaffolds constructed with 18-gauge ports performed the best out of the experimental groups, nearly reaching the tensile strength of the 200 mg/mL control group. Aside from the obvious visual differences between the groups, there was a statistical difference between the integrated scaffolds (18G port) and the laminated scaffolds, thus validating our hypothesis that integrated scaffolds would prove to be mechanically superior to laminated scaffolds.

The strain data provided an interesting observation: despite being electrospun at the lowest possible setting and producing what appeared to be a completely random scaffold, the strain data seems to be skewed towards greater perpendicular strains, hinting at the likelihood of a small degree of alignment. In each case the "perpendicular" component of the scaffolds, referring to scaffolds being stressed at an orientation 90 degrees from the direction of rotation of the target drum. This likens to pulling "against the grain" and in cases of high alignment leads to high strain levels and low stress levels. We did not detect any statistical difference between the two orientations in stress but there does exist statistical strain differences between test orientation in all scaffolds less the 100 mg/mL control, which shrunk after electrospinning so that alternate orientations couldn't be colleted, and the integrated scaffolds manufactured with 18G ports. While there was no statistical difference in the integrated scaffolds (18G port) there does appear to be a slight skew towards the perpendicular orientation.

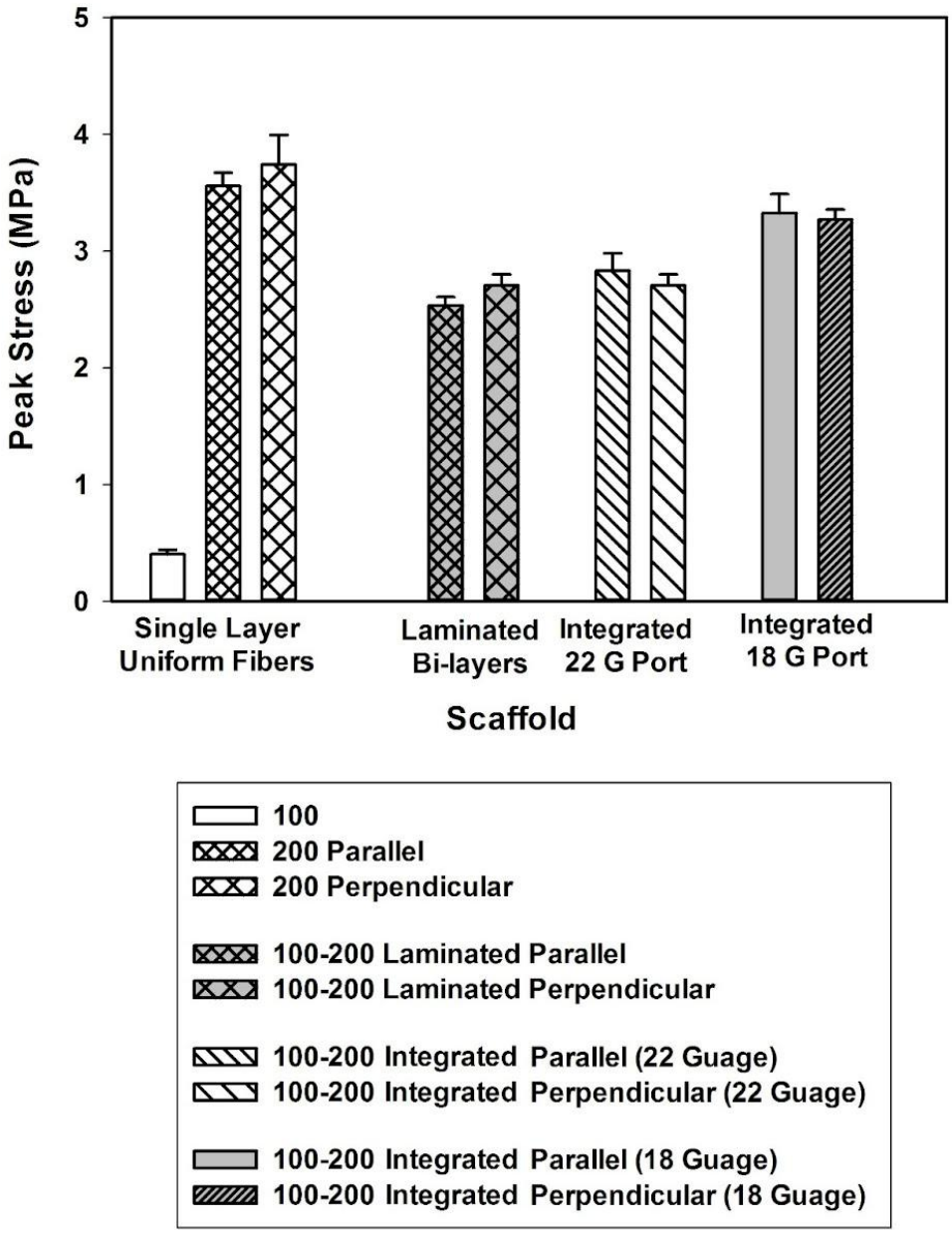


| | | | | |
|---|---|---|---|---|
| 200 Perpendicular vs. 100 | 3.314 | 13.436 | <0.001 | Yes |
| 200 paralle vs. 100 | 3.131 | 12.693 | <0.001 | Yes |
| Integrated vs. 100 | 2.934 | 12.439 | <0.001 | Yes |
| Integrated vs. 100 | 2.879 | 12.204 | <0.001 | Yes |
| Integrated vs. 100 | 2.406 | 9.755 | <0.001 | Yes |
| Integrated vs. 100 | 2.309 | 8.916 | <0.001 | Yes |
| Laminated Pe vs. 100 | 2.309 | 8.916 | <0.001 | Yes |
| Laminated parellel vs. 100 | 2.137 | 8.252 | <0.001 | Yes |
| 200 Perpendi vs. Laminated pa | 1.177 | 5.207 | <0.001 | Yes |
| 200 Perpendi vs. Laminated Pe | | | | |
| 200 Perpendi vs. Integrated | 0.908 | 4.284 | 0.005 | Yes |
| Integrated vs. Laminated pa | 0.798 | 3.723 | 0.020 | Yes |
| 200 paralle vs. Laminated Pe | 0.822 | 3.636 | 0.024 | Yes |
| 200 paralle vs. Integrated | 0.822 | 3.636 | 0.023 | Yes |
| Integrated vs. Laminated pa | 0.742 | 3.464 | 0.034 | Yes |
| 200 paralle vs. Integrated | 0.725 | 3.420 | 0.036 | Yes |

Fig. 36 Peak Stress Results from Tensile Testing.

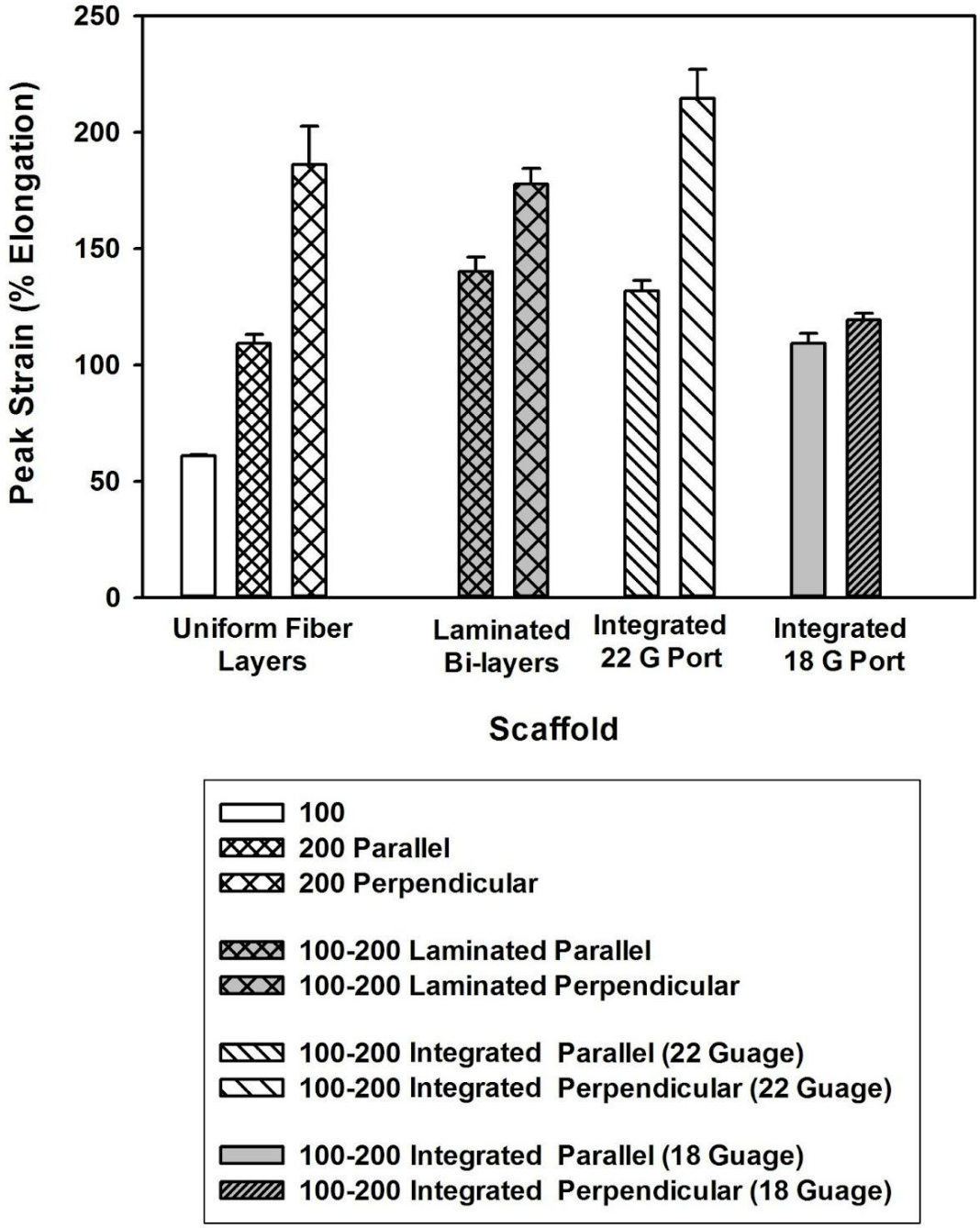


Fig. 37 Strain at Failure Results from Tensile Testing.

The stress-strain curves from tensile testing of the electrospun scaffolds, seen in Figures 38-41, show the different failure characteristics of each scaffold type. The 100-200 mg/mL integrated electrospinning scaffold (Figure 38, Figure 41 far left) shows that the scaffold experiences a positive linear stress-strain relationship before failure. The 100-200 mg/mL laminated electrospun scaffold (Figure 40, Figure 41 far right) shows that the scaffold undergoes a prolonged failure period after the linear stress-strain region and before total scaffold failure. The reason for the graphical difference is that the laminated scaffolds undergo biphasic failure, the 100 mg/mL section fails at the initial peak, leaving only the 200 mg/mL section as the load-bearing element of the scaffold (hence the immediate dip in stress). The scaffold still resists failure until the 200 mg/mL region finally fails, at which point the entire scaffold has failed. The 100-200 mg/mL semi-integrated electrospun scaffold, produced using a 22-gauge channel (Figure 39, Figure 41 middle), displays a failure graph somewhat in between the two extremes. The semi-integrated technique limits mixing and acts as an approximation of the laminated technique less the time interval between spinning required to exchange syringes.

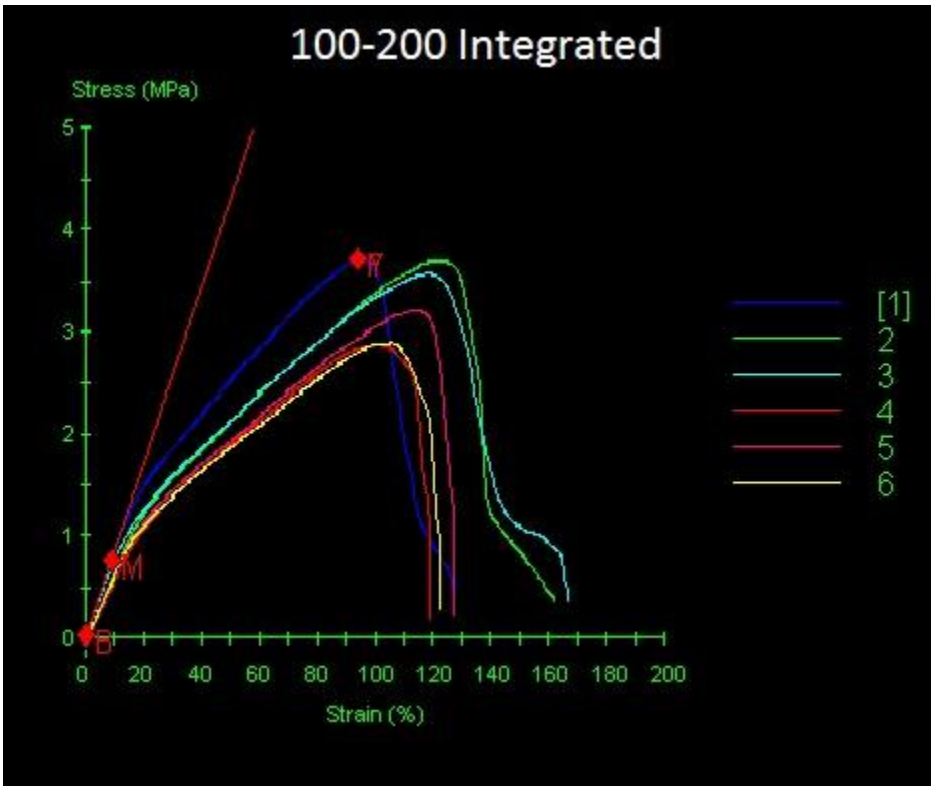


Fig. 38  Stress-strain graph for integrated scaffolds.

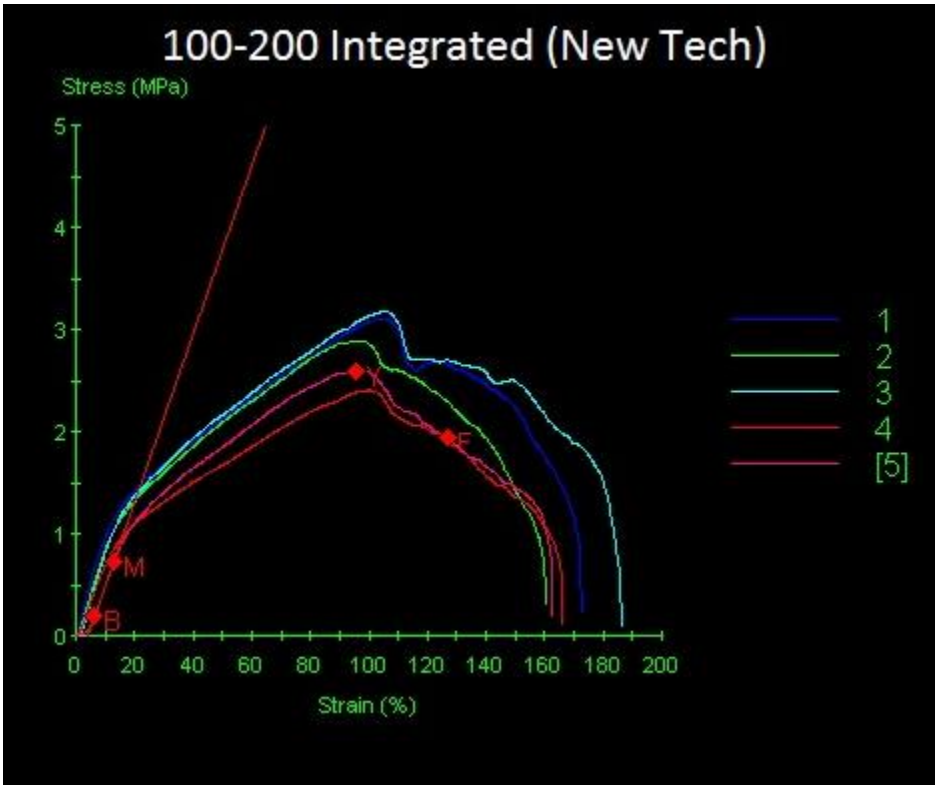

Fig. 39  Stress-strain graph for scaffold manufactured with the integrated electrospinning technique that approximates a laminated scaffold.

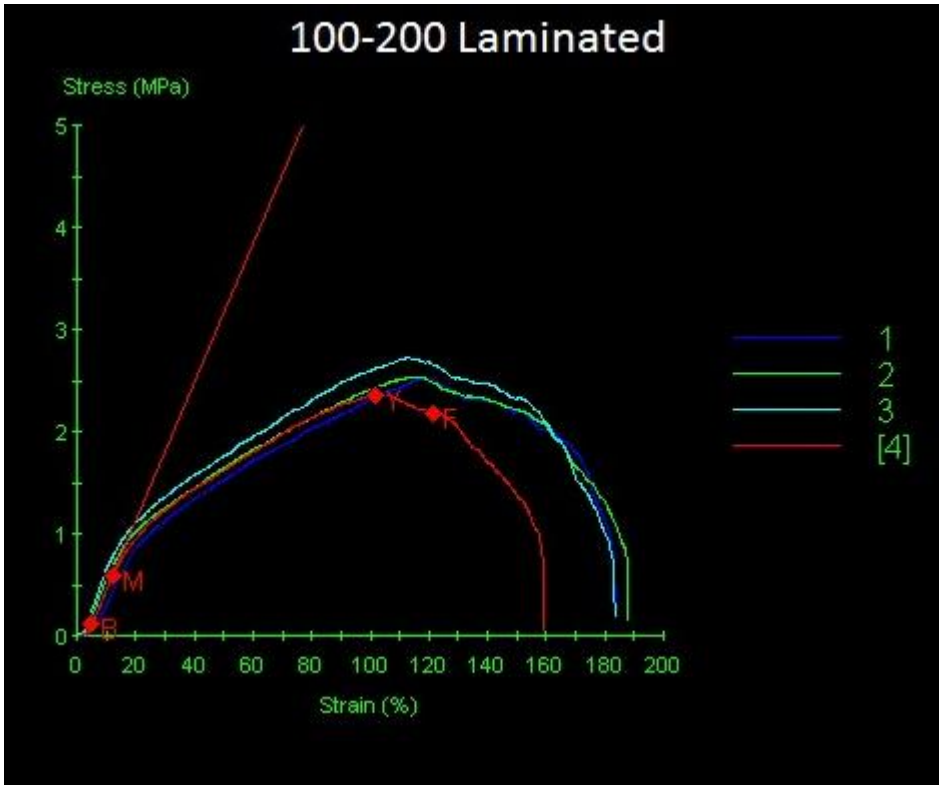


Fig. 40  Stress-strain graph for purely laminated scaffolds.

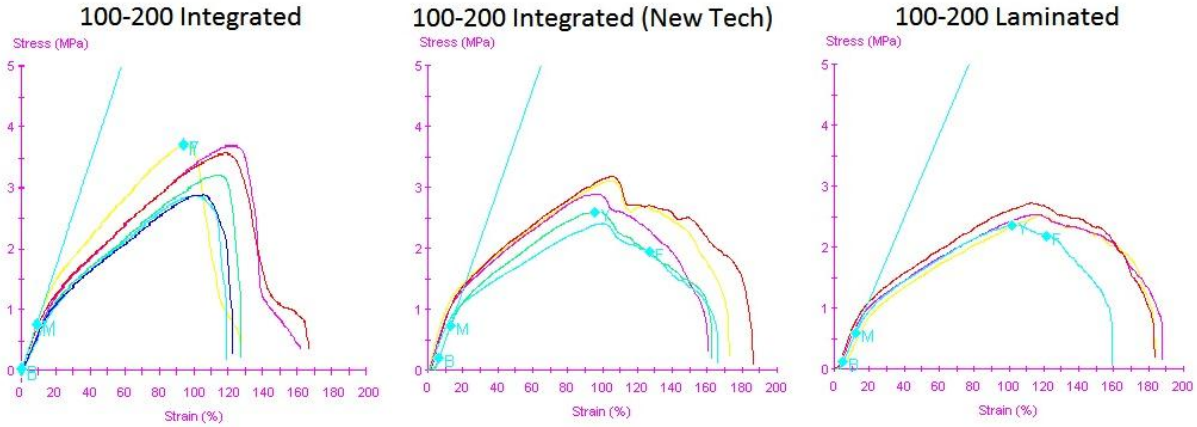

Fig. 41 Tensile test stress-strain graph for integrated fiber electrospinning (left), laminate approximating integrated fiber electrospinning (middle), and laminated scaffolds (right) Scaffolds. Note the differences in graph shape and failure modes. Comparing the three graphs side-by-side highlights the differences in failure mode. Colors were inverted for graphical clarity.

Integrated scaffolds failed at an average strain of 117% and, on average, achieved 17% additional strain before failure after peak stress. Semi-integrated scaffolds (approximating laminated scaffolds) and laminated scaffolds failed at average strains of 169% and 214%, respectively. They achieved respective averages of 69% and 83% additional strain before failure after peak stress. These observations are summarized in Table 1 below. The failure modes of these scaffolds were completely different as the integrated scaffold failed as a unified structure whereas the other two (integrated - laminated approximate and laminated scaffolds) both failed biphasically. In the laminated structures the layer of 100 mg/mL PCL, possessing less elasticity, fails at lower strains than the 200 mg/mL layer, which is more elastic. We can deduce several things about laminated scaffolds from their failure modes which involves failure in the 100 mg/mL layer and exposure of a pure 200 mg/mL layer before total scaffold failure. First, the stress-strain curve dips after the peak stress value, this symbolizes the first phase of the biphasic failure in which the 100 mg/mL layer fails, leaving only the 200 mg/mL layer intact, thus the drop in total stress occurs because there is physically less scaffold resisting force. Second, the scaffold does not immediately fail after the 100 mg/mL layer fails, so we know the remaining stress-strain characteristics are almost entirely due to a residual layer of 200 mg/mL scaffold (additionally we know the stress value may no longer be accurate because the cross-sectional area has been reduced).

By integrating the changes in fibers this biphasic failure mode can be mitigated. In our study we accomplished this by instigating a controlled transition between the fiber types.

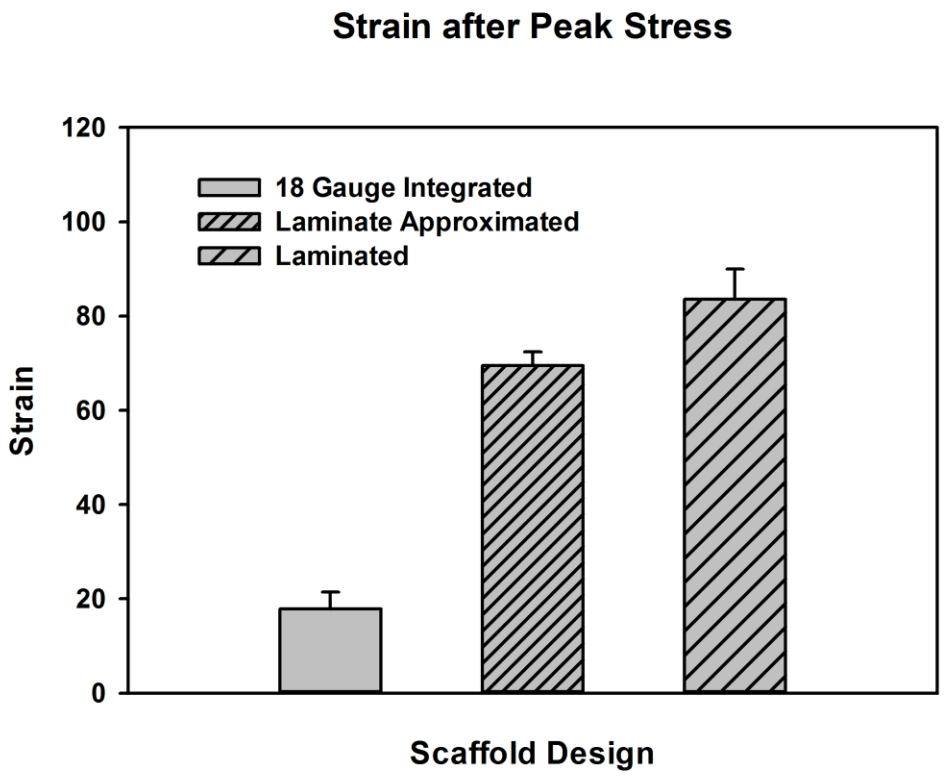


Fig. 42 Tensile Testing Failure Characteristics.

Through scanning electron microscopy we were able to analyze the failure characteristics of electrospun scaffolds. Figure 43 depicts a laminated electrospun scaffold section displaying very obvious signs of delamination after tensile testing to near failure. Because the fibrous layers aren't truly mechanically connected load is not adequately communicated through the boundary between layers. The result of this is a

biphasic failure where the 100 mg/mL layer begins to fail sooner than the 200 mg/mL layer, splitting apart to leave gaping holes in the scaffold (these are actually visible with the naked eye during tensile testing).

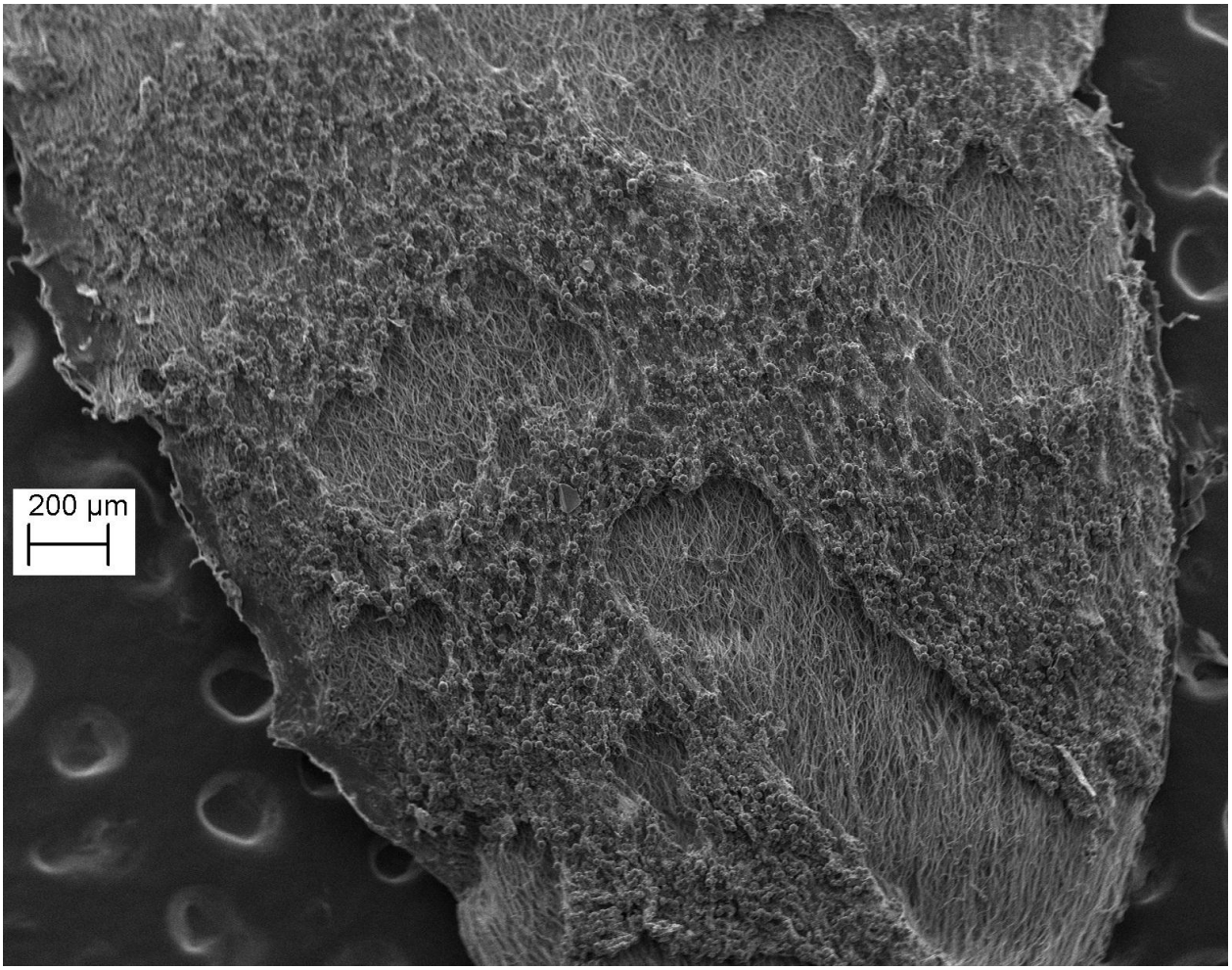


Fig. 43 SEM Image of Laminated Scaffold Stretched to Near Failure. Note the “islands” of delaminated fibers present on the surface.

In contrast to laminated structures, integrated fiber electrospinning produces a structure that fails in a much more unified way. Figure 44 depicts an integrated fiber

electrospinning scaffold after tensile testing to near failure. Note the lack of obvious delamination as the fibrous layers are mechanically well-connected and thus the load is able to be transferred throughout the scaffold. With the exception of the failure zone, the entire surface is composed of a continuous layer of small diameter fibers overlaying the larger diameter fibers.

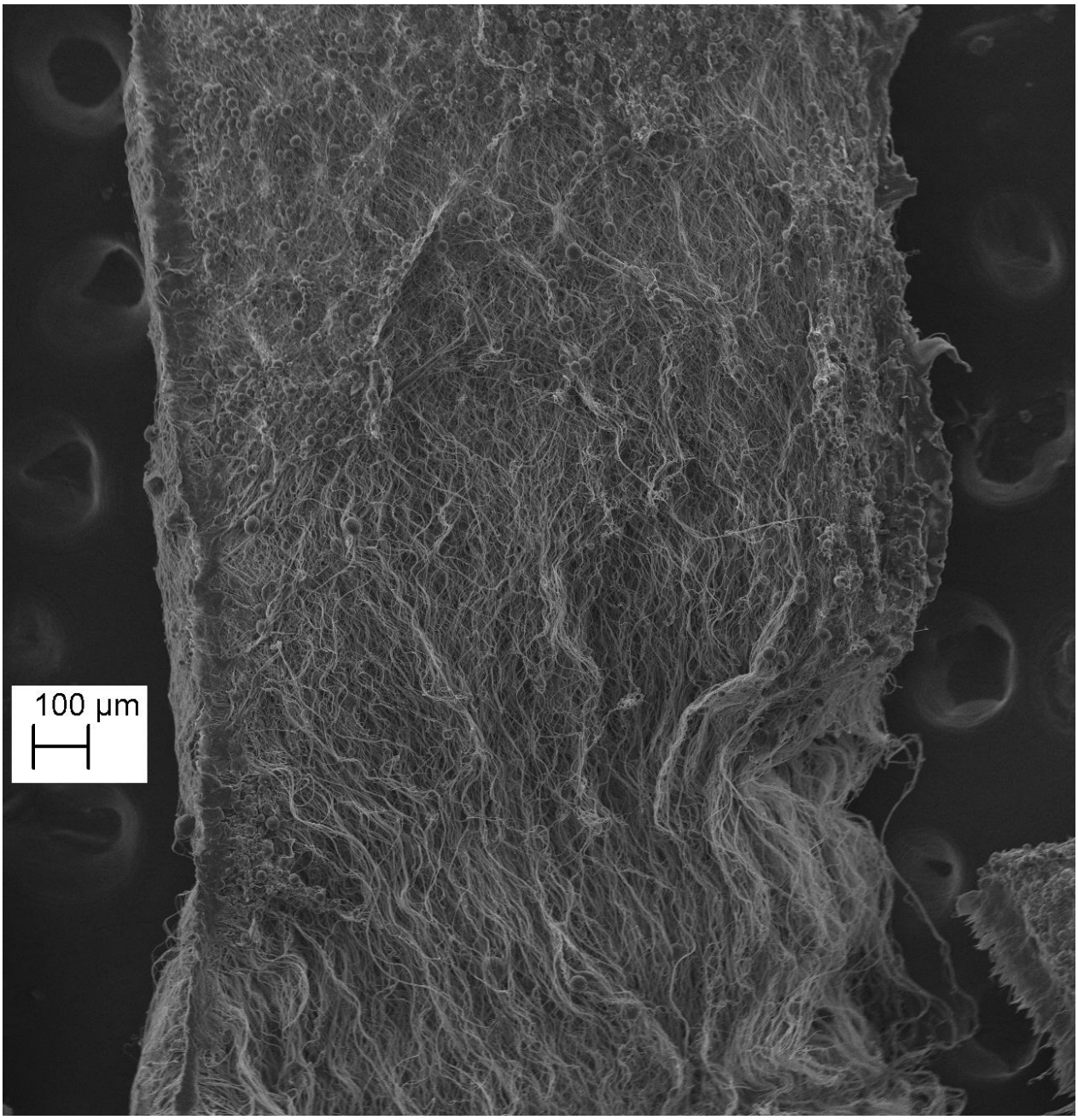

Fig. 44 SEM Image of Integrated Fiber Electrospinning Scaffold Stretched to 130% Strain (Near Failure).

### 3.3 Burst Testing

Electron microscopy reveals the different post-failure scaffold structures between electrospun scaffolds manufactured with our integrated fiber electrospinning technique and laminated scaffolds. Figure 45 contains images of electrospun scaffolds after burst testing. The entire integrated scaffold appeared like the segment shown on the left in Figure 45, thin fibers intermixed with beads. In contrast finding sections of 100 mg/mL PCL on the laminated scaffold was a challenge as the entire layer appears to have been obliterated. At a frequency of two to three per scaffold, “islands” of 100 mg/mL were found still attached to the 200 mg/mL layer of the laminated scaffolds. These SEM images depict the obvious differences in failure mode between the two electrospun scaffolds.

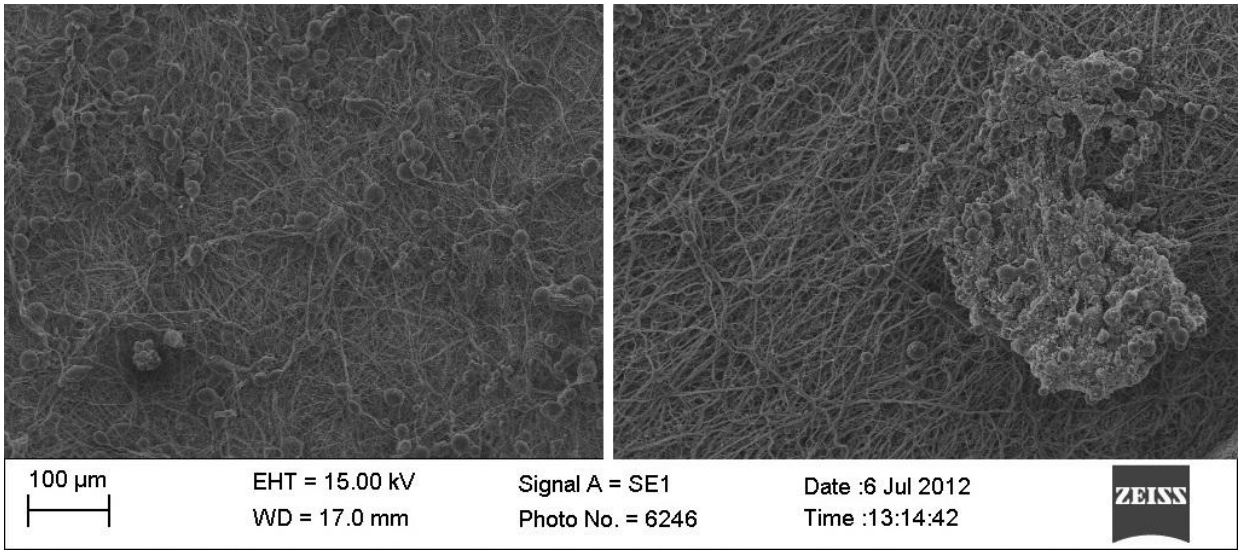

Fig. 45 SEM Images of the 100 mg/mL Face of the Integrated Fiber Electrospinning (Left) and Laminated (Right) Scaffolds After Burst Testing (200x).

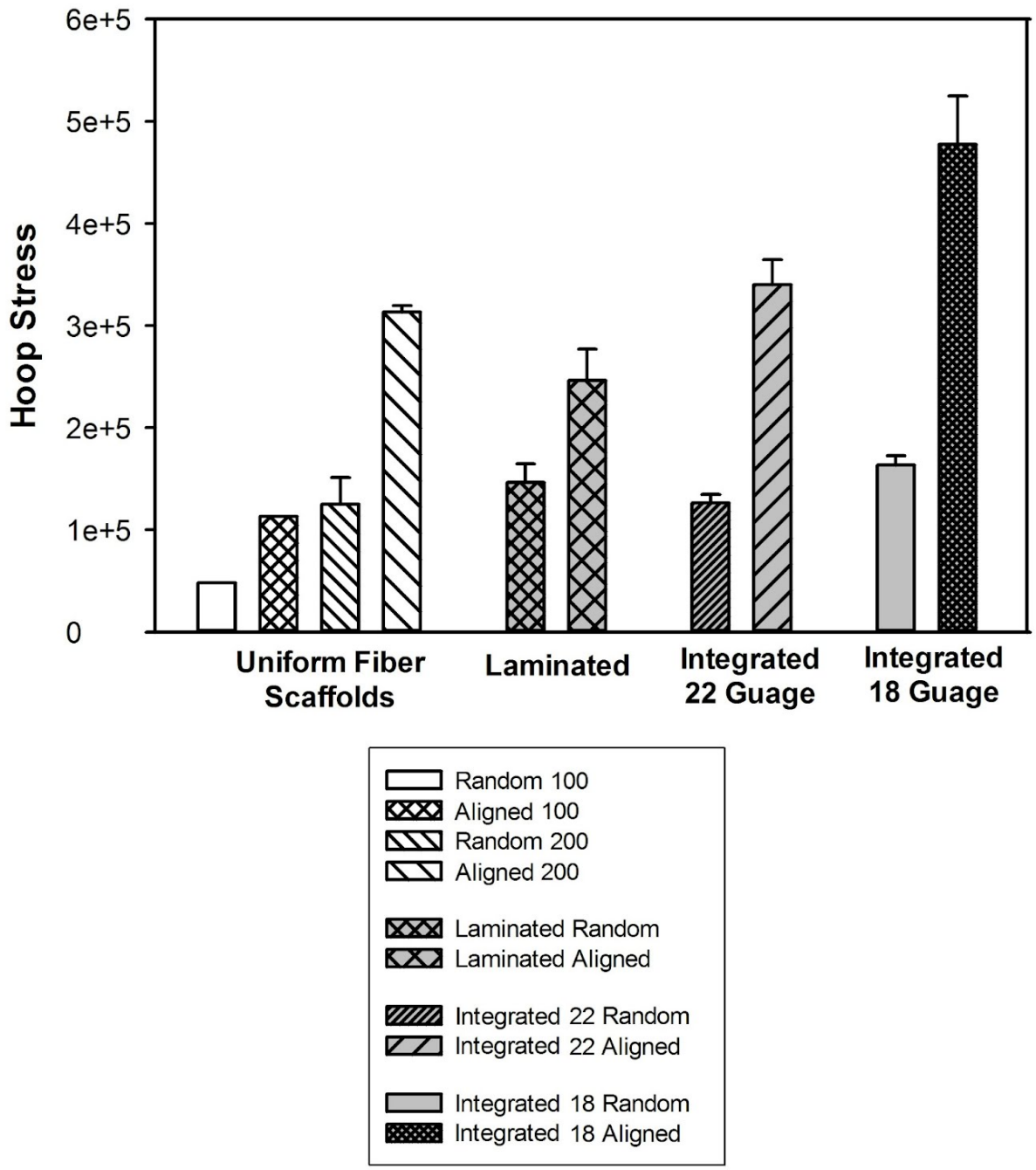


Fig. 46 Calculated Hoop Stress During Burst Testing.

### 3.4 Alignment Properties of Scaffolds at Failure

An interesting aspect of failure noted in this study was the tendency of fibrous scaffolds to align before failing (Figure 47). This was most prevalent in scaffolds containing pure 200 mg/mL PCL. Fast Fourier Transform analysis of this phenomenon is also shown in Figure 47.

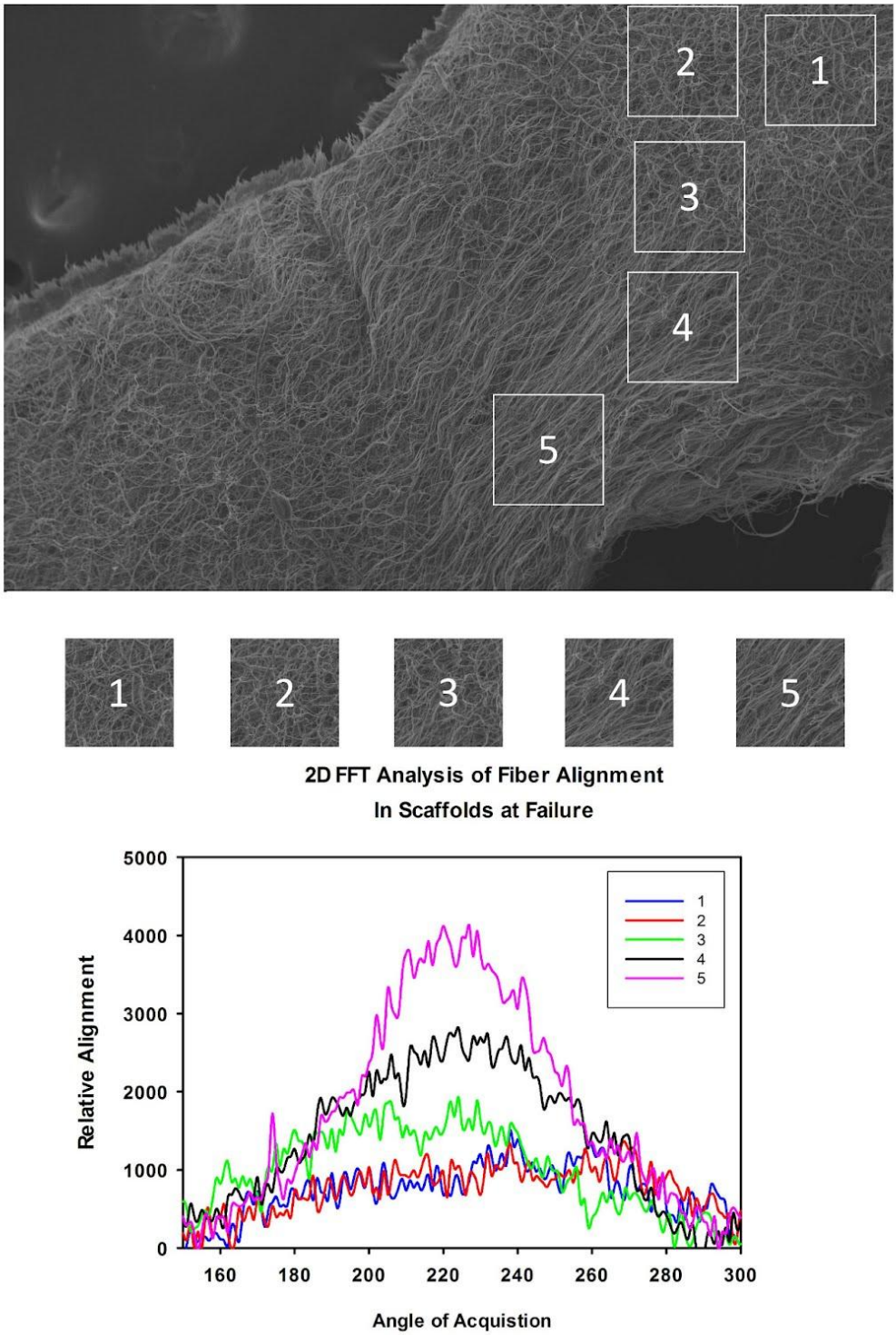


Fig. 47  Fiber alignment during failure and corresponding FFT.

# Chapter 4

# Discussion

## 4.1 Integrated Fiber Electrospinning Mixing Characteristics

The initial hypothesis regarding the spinning and mixing characteristics of the integrated fiber electrospinning system was that the intermediate plunger would travel down the length of the syringe in synchrony with the main plunger. While the two separate fluids would, for the most part, stay separate, they would mix slightly at the interface, leading to a relatively fast transition between the fluids and thus the fiber types. The scaffold we imagined would be produced would consist of two distinct layers with a brief, controlled transition joining them. What we noticed when we started experimenting with this technique was the inadequacy of the force on the intermediate plunger. Instead of moving in synchrony with the main plunger the intermediate plunger remained stationary until the the main plunger came into contact with it, at which point it was forced down the body of the syringe. This property of the integrated fiber electrospinning design changed the entire mode of fluid mixing as we hypothesized it; instead of possessing a small boundary layer at the plunger interface the second fluid was flowing freely into the first compartment where it mixed with the first fluid. Additionally this introduces several new variables to consider when analyzing the mixing of the two fluids. The intermediate channel now plays a role in mixing because its

diameter directly affects fluid velocity, which naturally affects the mixing properties of the system. Because the two fluids used in this study were of different viscosities, additional computational complexities were surely added to the system. Finally, as the fluids mix all of the flow characteristics become dynamic, further adding computational complexity to the system.

Despite inconsistencies with our hypothesis, the actual mixing characteristics of the integrated fiber electrospinning system, experimentally determined through dry weight polymer analysis and electrospun fiber analysis, were nearly ideal. In both cases the solution transitioned from low concentration/small fibers to high concentration/large fibers and did so over a period of several minutes, ensuring a smooth gradient unifying the overall scaffold. Using a smaller-gauge needle section through the intermediate plunger appeared to smooth out the mixing characteristics, however, the peak concentration/fiber size attained did not match what was achieved using the larger 18-gauge needle section through the intermediate plunger. Additionally the integrated scaffolds manufactured with the 18-gauge intermediate section mechanically outperformed those manufactured with 22-gauge intermediate sections.

In all cases the integrated fiber electrospinning system produced a tail off in polymer concentration/fiber diameter in the last few minutes of experimentation. We believe the reason for this is residual low concentration solution along the peripheries of the syringe. During testing we hypothesize that mixing takes place near the center of the syringe body as that is where the intermediate plunger outlet lies. The mixing dynamics of the syringe could produce a decreasing gradient of mixing closer to the periphery of the syringe body, leaving largely unaltered low concentration solution on

the syringe boundaries. As the primary plunger depresses further it physically pushes this low concentration fluid downward towards the syringe outlet and, toward the end of spinning, it starts to encompass a bulk of the remaining solution until it finally exits the system having decreased the overall polymer concentration/fiber diameter. This tail off in polymer concentration/fiber diameter could be mitigated through several techniques: Increasing the volume of the second electrospinning fluid, spreading the communicating channels throughout the intermediate disk, vibration application to the syringe body, thermal application to the syringe body (both vibration and thermal application to increase fluid flow and thus mixing), adjusting plunger velocities, and adjusting plunger architecture (concave towards the proximal solution as opposed to convex, this would encourage fluid flow from the periphery towards the center of the syringe body).

In contrast to the integrated fiber electrospinning system the laminated inherently produces no gradient in polymer concentration/fiber diameter. Because the solutions are kept separate there is no opportunity for mixing, resulting in a dynamic but non-unified structure that was found to fail in a predictable delaminating fashion.

## 4.2 Tensile Testing

### 4.2.1 Low Drum Rotational Speed (Non-Aligned Scaffolds) - Parallel, Perpendicular Comparison

Tensile testing involved imparting a set rate of deformation to the experimental scaffolds. With the rate of strain held constant the load varied depending on a scaffold's ability to withstand stress. In our tests the maximum stress values for the different

scaffolds were evaluated in two orientations, one parallel to the direction of collector drum rotation and one perpendicular to the direction of collector drum rotation. In stress testing neither orientation proved to be significantly different compared to its counterpart tested at a 90 degree skew. The results for strain to failure, however, showed a tendency for the perpendicular scaffolds to possess a larger overall strain before total scaffold failure. The strain results point to subtle degrees of alignment despite the slow rotational velocity of the drum collector as highly aligned scaffolds tend to resist stress best along the direction of the fibers and resist failure as a function of strain when tested at a 90 degree angle to the direction of fiber orientation. This finding is important because it brings to light that subtle changes in fiber alignment can produce very noticeable changes in mechanical properties. Because of this fact the comparisons will be limited to those of the same fiber orientation, even in “random” scaffolds. It should also be noted that the difference in strain between parallel and perpendicular configurations of integrated scaffolds with 18-gauge intermediate channels was negligible. It’s possible that the more erratic changes in polymer concentration, as seen in the dry weight analysis, produce a more erratic and random fibrous structure. Because a completely randomly aligned structure would have no directional preference the strain and stress results should be the same regardless of the orientation of testing.

### 4.2.2 Low Drum Rotational Speed (Non-Aligned Scaffolds) - Electrospinning Method Stress Comparison

The integrated scaffolds, especially the ones made with 18-gauge intermediate channels, showed higher peak stress values than laminated scaffolds, approaching the

values for the 200 mg/mL control group. While it isn't obvious by simply looking at the peak stress values for each method, the modes of failure for the different types of scaffold are tremendously different, leading to not only different peak stress values but also to vastly different stress-strain curves. Laminated scaffolds approximate two separate scaffolds tested in parallel and, when both of the scaffolds are intact, they resist stress very much like the integrated scaffolds. Where the laminated scaffolds start to diverge is when the 100 mg/mL layer fails, instigating a very noticeable decrease in stress, but not complete scaffold failure (unlike the burst tests). Once the 100 mg/mL layer fails the stress dips because the only resistive element in the scaffold is the remaining 200 mg/mL section, which does resist load for a considerable time after the failure of the 100 mg/mL layer. This biphasic failure is characteristic of any structure consisting of unjoined or weakly joined laminated materials with different material properties. In contrast, the integrated scaffolds failure much more like a scaffold manufactured from a single fiber type. This is because the fibers transition smoothly so that the stress is distributed throughout that scaffold and localized failures do not encompass a majority of the scaffold. In this way the integrated scaffolds do not experience biphasic failure and make a mechanically more desirable product.

### 4.3 Burst Testing

Unlike tensile testing where a variable force is applied to maintain a steady rate of strain, burst testing involves incrementally increasing radial force until scaffold failure occurs. In burst testing there is no opportunity for a scaffold with biphasic failure tendencies to recover after the initial layer failure. The failure of laminated scaffolds in

burst testing, because of their biphasic failure nature, is seen as an immediate and catastrophic scaffold failure. Laminated scaffolds, under increasing radial pressure, expand to the degree dictated by the least-expandable element in its structure, in this case the 100 mg/mL section. Once the first layer fails, exposing the second as the only force-resisting element in the structure, the scaffold fails almost immediately afterwards. This rapid successive failure is due to the fact that while the scaffold initially resists a large amount of stress as a unified structure, the 100 mg/mL layer starts to fail at low strain levels compared to the 200 mg/mL section. Once the 100 mg/mL layer fails the remaining scaffold is comparatively less-thick than the original scaffold and, as such, unable to withstand the forces imparted on it by the burst test.

In this study we found that the integrated fiber electrospinning technique produced scaffolds with much higher burst testing capabilities than laminated scaffolds. The integrated scaffolds did not experience the catastrophic biphasic failure as with laminated scaffolds and were able to withstand more radial stress.

# Chapter 5

## Conclusions

In our study the integrated fiber electrospinning system produced scaffolds that were mechanically superior to laminated scaffolds. This novel electrospinning technique produced scaffolds that incorporated multiple fiber types integrated into a single, unified structure. We conclusively proved that scaffolds manufactured in a laminated form possess a biphasic failure mode whereas scaffolds manufactured with our novel integrated fiber electrospinning technique possessed a failure mode similar to that of a scaffold composed of a single fiber type. This combination of ideal failure mode, increased tensile strength, increased burst pressure, and a smooth structural gradient make our novel integrated fiber electrospinning scaffolds superior to any other multiple-fiber scaffold produced with conventional electrospinning techniques.

## Chapter 6

## Future Work and Other Discussion

Tissue engineering focuses on manufacturing a scaffold that completely replicates the functioning tissue. It may be that the ideal tissue regeneration environment is not the perfectly replicated “empty shell” of a functional tissue but another type of graft, by itself nothing like a functional tissue but infused with the correct factors to induce ECM formation which, in turn, initiates the “regenerative cascade” if you will, by which the body will naturally progress into functional tissue. We seem to focus too much on creating a scaffold that looks and feels like a functional tissue as opposed to setting the body up with the best possible regenerative environment.

By placing a load cell in series with the syringe driver plate and the plunger the viscosity of the solution can be monitored over time. This method could be programmable with the following variables (to name a few): polymer, polymer concentration (not completely necessary, maybe just as a check for the force, could tell you if there’s a problem with the capillary tube), solvent, capillary tube ID, flow rate, distance to target, and dispensing force (as measured by the load cell). With these variables it should be possible to create a platform that varies the electrical potential of the system to optimize the electrospinning process.

Strategically varying the atmospheric solvent concentration in an electrospinning system may make it possible to create a gradient in crystallinity in a structure. This may be useful in drug delivery systems as degradation rate of scaffolds could be engineered to be dynamic. The basic premise behind this idea is that highly-crystalline structures dissolve at a lower rate than less-crystalline structures. An example of this could be a spherical implantable drug-delivery platform where the goal was to maintain the overall volume of drug delivery. This could theoretically be attained by initiating electrospinning with a low atmospheric solvent concentration (or even directly removing all atmospheric solvent), thus instigating lower fiber crystallinity. Electrospinning would then progress with an increasing atmospheric solvent concentration to instigate higher fiber crystallinity. In this way a structure could be manufactured with progressively less crystallinity as it dissolves. It's possible to balance the decreasing surface area with an increase in dissolution rate in order to maintain a constant volume of drug delivery.

## Appendix

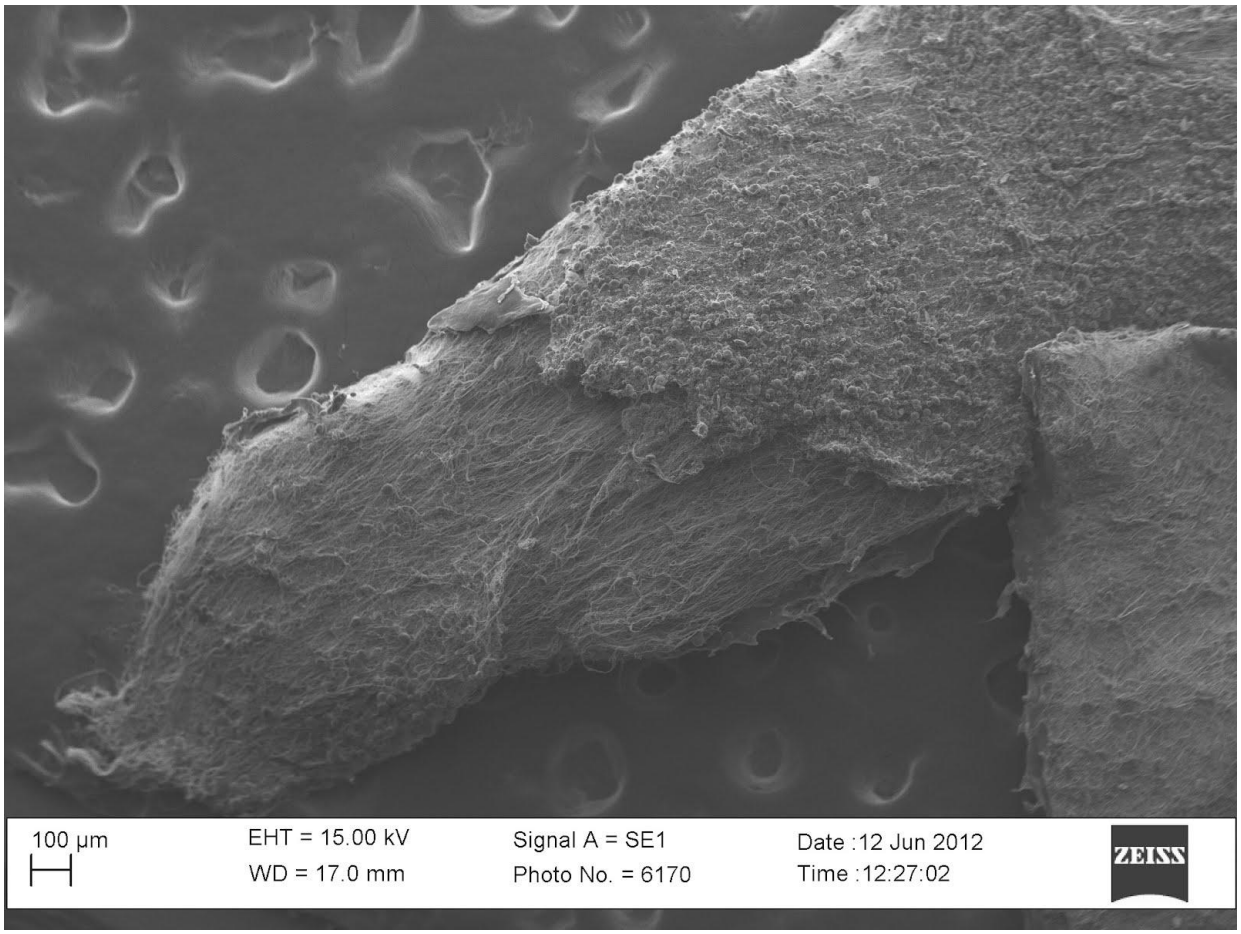


Fig. 48 Example of a laminated scaffold after tensile failure.

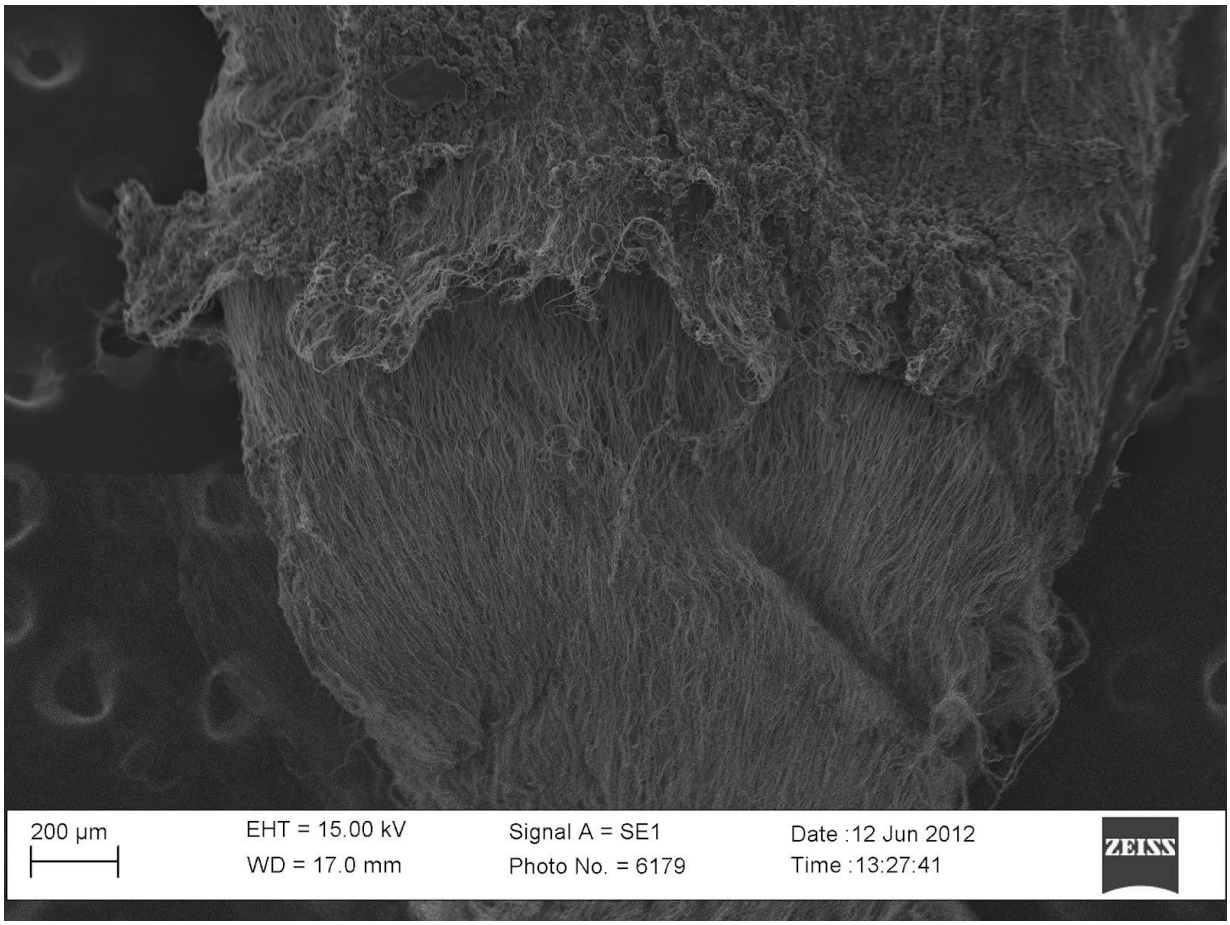


Fig. 49  Example of a laminated scaffold after tensile failure.

**One Way Repeated Measures Analysis of Variance** Thursday, July 26, 2012, 3:57:32 PM

**Data source:** Peak Stress for aligned Scaffolds in casey stress aligned data

**Normality Test (Shapiro-Wilk)** Passed (P = 0.839)

**Equal Variance Test:** Failed (P < 0.050)

| Treatment Name | N | Missing | Mean | Std Dev | SEM |
|---|---|---|---|---|---|
| Laminated parellel | 4 | 0 | 9.683 | 0.635 | 0.317 |
| Laminated Perpendicular | 4 | 0 | 1.423 | 0.0548 | 0.0274 |
| paral aligned 18 guage | 2 | 0 | 8.375 | 2.140 | 1.513 |
| perpend 18 guage | 6 | 0 | 1.319 | 0.0822 | 0.0335 |

| Source of Variation | DF | SS | MS | F | P |
|---|---|---|---|---|---|
| Between Subjects | 5 | 2.144 | 0.429 | | |
| Between Treatments | 3 | 210.672 | 70.224 | 133.376 | <0.001 |
| Residual | 7 | 3.686 | 0.527 | | |
| Total | 15 | 241.353 | 16.090 | | |

The differences in the mean values among the treatment groups are greater than would be expected by chance; there is a statistically significant difference (P = <0.001). To isolate the group or groups that differ from the others use a multiple comparison procedure.

Power of performed test with alpha = 0.050: 1.000

Expected Mean Squares:
Approximate DF Residual = 7.000
Expected MS(Subj) = var(res) + 2.400 var(Subj)
Expected MS(Treatment) = var(res) + var(Treatment)
Expected MS(Residual) = var(res)

All Pairwise Multiple Comparison Procedures (Holm-Sidak method):
Overall significance level = 0.05

Comparisons for factor:

| Comparison | Diff of Means | t | P | P<0.050 |
|---|---|---|---|---|
| Laminated pa vs. perpend 18 g | 8.357 | 16.287 | <0.001 | Yes |
| Laminated pa vs. Laminated Pe | 8.259 | 13.941 | <0.001 | Yes |
| paral aligne vs. perpend 18 g | 7.028 | 10.611 | <0.001 | Yes |
| paral aligne vs. Laminated Pe | 6.931 | 9.552 | <0.001 | Yes |
| Laminated pa vs. paral aligne | 1.328 | 1.830 | 0.208 | No |
| Laminated Pe vs. perpend 18 g | 0.0970 | 0.189 | 0.855 | No |

Fig. 50 Stress Statistics (Aligned).

**One Way Repeated Measures Analysis of Variance** Tuesday, July 24, 2012, 3:24:13 PM

**Data source:** Peak Stress for all Scaffolds in Casey materials stess testingA

**Normality Test (Shapiro-Wilk)** Passed (P = 0.392)

**Equal Variance Test:** Failed (P < 0.050)

| Treatment Name | N | Missing | Mean | Std Dev | SEM |
|---|---|---|---|---|---|
| 100 | 3 | 0 | 0.406 | 0.0621 | 0.0358 |
| 200 paralle | 5 | 0 | 3.558 | 0.254 | 0.114 |
| 200 Perpendicular | 5 | 0 | 3.741 | 0.572 | 0.256 |
| Laminated parellel | 4 | 0 | 2.534 | 0.148 | 0.0742 |
| Laminated Perpendicular | 4 | 0 | 2.706 | 0.191 | 0.0956 |
| 22 parallel | 5 | 0 | 2.833 | 0.329 | 0.147 |
| 22 perpendicular | 4 | 0 | 2.706 | 0.191 | 0.0956 |
| 18 parallel | 6 | 0 | 3.326 | 0.395 | 0.161 |
| 18 perpendicular | 6 | 0 | 3.271 | 0.206 | 0.0839 |

| Source of Variation | DF | SS | MS | F | P |
|---|---|---|---|---|---|
| Between Subjects | 5 | 0.382 | 0.0763 | | |
| Between Treatments | 8 | 24.999 | 3.125 | 30.161 | <0.001 |
| Residual | 28 | 2.901 | 0.104 | | |
| Total | 41 | 30.373 | 0.741 | | |

The differences in the mean values among the treatment groups are greater than would be expected by chance; there is a statistically significant difference (P = <0.001). To isolate the group or groups that differ from the others use a multiple comparison procedure.

Power of performed test with alpha = 0.050: 1.000

Expected Mean Squares:
Approximate DF Residual = 28.000
Expected MS(Subj) = var(res) + 6.600 var(Subj)
Expected MS(Treatment) = var(res) + var(Treatment)
Expected MS(Residual) = var(res)

All Pairwise Multiple Comparison Procedures (Holm-Sidak method):
Overall significance level = 0.05

Comparisons for factor:

| Comparison | Diff of Means | t | P | P<0.050 |
|---|---|---|---|---|
| 200 Perpendicular vs. 100 | 3.314 | 13.436 | <0.001 | Yes |
| 200 paralle vs. 100 | 3.131 | 12.693 | <0.001 | Yes |
| 18 parallel vs. 100 | 2.934 | 12.439 | <0.001 | Yes |
| 18 perpendicular vs. 100 | 2.879 | 12.204 | <0.001 | Yes |
| 22 parallel vs. 100 | 2.406 | 9.755 | <0.001 | Yes |
| 22 perpendicular vs. 100 | 2.309 | 8.916 | <0.001 | Yes |
| Laminated Pe vs. 100 | 2.309 | 8.916 | <0.001 | Yes |
| Laminated parellel vs. 100 | 2.137 | 8.252 | <0.001 | Yes |
| 200 Perpendi vs. Laminated pa | 1.177 | 5.207 | <0.001 | Yes |
| 200 Perpendi vs. Laminated Pe | 1.005 | 4.446 | 0.003 | Yes |
| 200 Perpendi vs. 22 perpendic | 1.005 | 4.446 | 0.003 | Yes |
| 200 paralle vs. Laminated pa | 0.994 | 4.397 | 0.004 | Yes |
| 200 Perpendi vs. 22 parallel | 0.908 | 4.284 | 0.005 | Yes |
| 18 parallel vs. Laminated pa | 0.798 | 3.723 | 0.020 | Yes |
| 200 paralle vs. Laminated Pe | 0.822 | 3.636 | 0.024 | Yes |
| 200 paralle vs. 22 perpendic | 0.822 | 3.636 | 0.023 | Yes |
| 18 perpendic vs. Laminated pa | 0.742 | 3.464 | 0.034 | Yes |
| 200 paralle vs. 22 parallel | 0.725 | 3.420 | 0.036 | Yes |
| 18 parallel vs. Laminated Pe | 0.626 | 2.920 | 0.116 | No |
| 18 parallel vs. 22 perpendic | 0.626 | 2.920 | 0.110 | No |
| 18 perpendic vs. Laminated Pe | 0.570 | 2.661 | 0.186 | No |
| 18 perpendic vs. 22 perpendic | 0.570 | 2.661 | 0.175 | No |
| 18 parallel vs. 22 parallel | 0.528 | 2.652 | 0.168 | No |
| 18 perpendic vs. 22 parallel | 0.473 | 2.373 | 0.278 | No |
| 200 Perpendi vs. 18 perpendic | 0.435 | 2.182 | 0.369 | No |
| 200 Perpendi vs. 18 parallel | 0.379 | 1.904 | 0.535 | No |
| 200 paralle vs. 18 perpendic | 0.252 | 1.263 | 0.913 | No |
| 22 parallel vs. Laminated pa | 0.269 | 1.192 | 0.919 | No |
| 200 paralle vs. 18 parallel | 0.196 | 0.984 | 0.961 | No |
| 200 Perpendi vs. 200 paralle | 0.183 | 0.865 | 0.970 | No |
| 22 perpendic vs. Laminated pa | 0.172 | 0.718 | 0.980 | No |
| Laminated Pe vs. Laminated pa | 0.172 | 0.718 | 0.961 | No |
| 22 parallel vs. 22 perpendic | 0.0974 | 0.431 | 0.988 | No |
| 22 parallel vs. Laminated Pe | 0.0974 | 0.431 | 0.964 | No |
| 18 parallel vs. 18 perpendic | 0.0555 | 0.299 | 0.946 | No |
| 22 perpendic vs. Laminated Pe | 4.441E-016 | 1.855E-015 | 1.000 | No |

Fig. 51 Stress Statistics (Not Aligned).

**One Way Repeated Measures Analysis of Variance** Thursday, July 26, 2012, 10:44:22 AM

**Data source:** Peak Strain for aligned Scaffolds in casey strain aligned data

**Normality Test (Shapiro-Wilk)** Passed (P = 0.346)

**Equal Variance Test:** Passed (P = 0.590)

| Treatment Name | N | Missing | Mean | Std Dev | SEM |
|---|---|---|---|---|---|
| Laminated parellel | 4 | 0 | 92.825 | 7.120 | 3.560 |
| Laminated Perpendicular | 3 | 0 | 506.600 | 68.051 | 39.289 |
| paral aligned 18 guage | 2 | 0 | 81.100 | 2.546 | 1.800 |
| perpend 18 guage | 6 | 0 | 229.167 | 50.925 | 20.790 |

| Source of Variation | DF | SS | MS | F | P |
|---|---|---|---|---|---|
| Between Subjects | 5 | 12179.324 | 2435.865 | | |
| Between Treatments | 3 | 349258.361 | 116419.454 | 68.429 | <0.001 |
| Residual | 6 | 10207.957 | 1701.326 | | |
| Total | 14 | 371493.077 | 26535.220 | | |

The differences in the mean values among the treatment groups are greater than would be expected by chance; there is a statistically significant difference (P = <0.001). To isolate the group or groups that differ from the others use a multiple comparison procedure.

Power of performed test with alpha = 0.050: 1.000

Expected Mean Squares:
Approximate DF Residual = 6.000
Expected MS(Subj) = var(res) + 2.200 var(Subj)
Expected MS(Treatment) = var(res) + var(Treatment)
Expected MS(Residual) = var(res)

All Pairwise Multiple Comparison Procedures (Holm-Sidak method):
Overall significance level = 0.05

Comparisons for factor:

| Comparison | Diff of Means | t | P | P<0.050 |
|---|---|---|---|---|
| Laminated Pe vs. Laminated pa | 425.158 | 11.585 | <0.001 | Yes |
| Laminated Pe vs. paral aligne | 432.806 | 9.832 | <0.001 | Yes |
| Laminated Pe vs. perpend 18 g | 282.508 | 8.664 | <0.001 | Yes |
| perpend 18 g vs. Laminated pa | 142.650 | 4.891 | 0.008 | Yes |
| perpend 18 g vs. paral aligne | 150.297 | 3.959 | 0.015 | Yes |
| Laminated pa vs. paral aligne | 7.647 | 0.184 | 0.860 | No |

Fig. 52 Strain Statistics (Aligned).

**One Way Repeated Measures Analysis of Variance** Tuesday, July 24, 2012, 10:00:42 AM

**Data source:** Peak Strain for all Scaffolds in Casey strain materials testing

**Normality Test (Shapiro-Wilk)** Passed (P = 0.087)

**Equal Variance Test:** Passed (P = 0.141)

| Treatment Name | N | Missing | Mean | Std Dev | SEM |
|---|---|---|---|---|---|
| 100 | 2 | 0 | 61.050 | 0.778 | 0.550 |
| 200 parellel | 5 | 0 | 186.160 | 36.838 | 16.475 |
| 200 Perpendicular | 5 | 0 | 109.400 | 8.568 | 3.832 |
| Laminated parellel | 4 | 0 | 140.150 | 12.616 | 6.308 |
| Laminated Perpendicular | 4 | 0 | 177.850 | 13.112 | 6.556 |
| Integrated parallel 22 | 5 | 0 | 131.720 | 10.492 | 4.692 |
| Integrated Perpendicular 22 | 4 | 0 | 214.500 | 25.016 | 12.508 |
| Integrated parallal 18 | 6 | 0 | 109.333 | 10.856 | 4.432 |
| Integrated perpendicular 18 | 6 | 0 | 119.350 | 7.193 | 2.936 |

| Source of Variation | DF | SS | MS | F | P |
|---|---|---|---|---|---|
| Between Subjects | 5 | 1858.935 | 371.787 | | |
| Between Treatments | 8 | 63912.587 | 7989.073 | 26.888 | <0.001 |
| Residual | 27 | 8022.498 | 297.130 | | |
| Total | 40 | 74148.390 | 1853.710 | | |

The differences in the mean values among the treatment groups are greater than would be expected by chance; there is a statistically significant difference (P = <0.001). To isolate the group or groups that differ from the others use a multiple comparison procedure.

Power of performed test with alpha = 0.050: 1.000

Expected Mean Squares:
Approximate DF Residual = 27.000
Expected MS(Subj) = var(res) + 6.400 var(Subj)
Expected MS(Treatment) = var(res) + var(Treatment)
Expected MS(Residual) = var(res)

All Pairwise Multiple Comparison Procedures (Holm-Sidak method):
Overall significance level = 0.05

Comparisons for factor:

| Comparison | Diff of Means | t | P | P<0.050 |
|---|---|---|---|---|
| Integrated vs. 100 | 156.206 | 9.920 | <0.001 | Yes |
| Integrated vs. Integrated | 108.364 | 9.442 | <0.001 | Yes |
| Integrated vs. 200 Perpendi | 108.156 | 8.933 | <0.001 | Yes |
| Integrated vs. Integrated | 98.348 | 8.569 | <0.001 | Yes |
| 200 paralle vs. 100 | 124.810 | 8.227 | <0.001 | Yes |
| Laminated Pe vs. 100 | 119.556 | 7.592 | <0.001 | Yes |
| 200 paralle vs. Integrated | 76.968 | 7.212 | <0.001 | Yes |
| Integrated vs. Integrated | 85.836 | 7.090 | <0.001 | Yes |
| 200 paralle vs. 200 Perpendi | 76.760 | 6.765 | <0.001 | Yes |
| 200 paralle vs. Integrated | 66.952 | 6.273 | <0.001 | Yes |
| Laminated Pe vs. Integrated | 71.714 | 6.248 | <0.001 | Yes |
| Laminated Pe vs. 200 Perpendi | 71.506 | 5.906 | <0.001 | Yes |
| Integrated vs. Laminated pa | 74.350 | 5.798 | <0.001 | Yes |
| Laminated Pe vs. Integrated | 61.698 | 5.376 | <0.001 | Yes |
| Laminated parellel vs. 100 | 81.856 | 5.198 | <0.001 | Yes |
| 200 paralle vs. Integrated | 54.440 | 4.798 | 0.001 | Yes |
| Integrated vs. 100 | 70.370 | 4.639 | 0.002 | Yes |
| Laminated Pe vs. Integrated | 49.186 | 4.063 | 0.007 | Yes |
| Integrated vs. 100 | 57.859 | 3.943 | 0.009 | Yes |
| 200 paralle vs. Laminated pa | 42.954 | 3.548 | 0.024 | Yes |
| Integrated vs. 100 | 47.842 | 3.261 | 0.047 | Yes |
| 200 Perpendicular vs. 100 | 48.050 | 3.167 | 0.055 | No |
| Laminated pa vs. Integrated | 34.014 | 2.964 | 0.084 | No |
| Laminated Pe vs. Laminated pa | 37.700 | 2.940 | 0.083 | No |
| Integrated vs. Laminated Pe | 36.650 | 2.858 | 0.093 | No |
| Laminated pa vs. 200 Perpendi | 33.806 | 2.792 | 0.100 | No |
| Integrated vs. 200 paralle | 31.396 | 2.593 | 0.142 | No |
| Integrated vs. Integrated | 22.528 | 2.111 | 0.334 | No |
| Laminated pa vs. Integrated | 23.998 | 2.091 | 0.314 | No |
| Integrated vs. 200 Perpendi | 22.320 | 1.967 | 0.349 | No |
| Integrated vs. Integrated | 12.512 | 1.172 | 0.824 | No |
| Integrated vs. Integrated | 10.017 | 1.006 | 0.858 | No |
| Laminated pa vs. Integrated | 11.486 | 0.949 | 0.823 | No |
| Integrated vs. 200 Perpendi | 9.808 | 0.919 | 0.745 | No |
| 200 paralle vs. Laminated Pe | 5.254 | 0.434 | 0.890 | No |
| 200 Perpendi vs. Integrated | 0.208 | 0.0195 | 0.985 | No |

Fig. 53 Strain Statistics (Not Aligned).

## Literature Cited

1 - Luiz H. Catalani, et al. "Charge Generation, Charge Transport, And Residual Charge In The Electrospinning Of Polymers: A Review Of Issues And Complications." Journal Of Applied Physics 111.4 (2012): 044701. Academic Search Complete. Web. 15 July 2012.

2 - Xiang-Fa, Wu, Yury Salkovskiy, and Yuris A. Dzenis. "Modeling Of Solvent Evaporation From Polymer Jets In Electrospinning." Applied Physics Letters 98.22 (2011): 223108. Computers & Applied Sciences Complete. Web. 16 July 2012.

3 - Darrell H. Reneker, Alexander L. Yarin, Hao Fong, and Sureeporn Koombhongse, Bending instability of electrically charged liquid jets of polymer solutions in electrospinning. J. Appl. Phys. 87, 4531 (2000), DOI:10.1063/1.373532

4 - Antonio Speranza, Mojtaba Ghadiri, Mark Newman, Libero Sesti Osseo, Giovanna Ferrari, Electro-spraying of a highly conductive and viscous liquid, Journal of Electrostatics, Volumes 51–52, May 2001, Pages 494-501.

5 - Carl B. Giller, D. Bruce Chase, John F. Rabolt, Christopher M. Snively, Effect of solvent evaporation rate on the crystalline state of electrospun Nylon 6, Polymer, Volume 51, Issue 18, 19 August 2010, Pages 4225-4230.

6 - Balendu S. Jha, Raymond J. Colello, James R. Bowman, Scott A. Sell, Kangmin D. Lee, John W. Bigbee, Gary L. Bowlin, Woon N. Chow, Bruce E. Mathern, David G. Simpson, Two pole air gap electrospinning: Fabrication of highly aligned, three-dimensional scaffolds for nerve reconstruction, Acta Biomaterialia, Volume 7, Issue 1, January 2011, Pages 203-215.

7 - Avinash Baji, Yiu-Wing Mai, Shing-Chung Wong, Mojtaba Abtahi, Pei Chen, Electrospinning of polymer nanofibers: Effects on oriented morphology, structures and tensile properties, Composites Science and Technology, Volume 70, Issue 5, May 2010, Pages 703-718.

8 - https://bcrc.bio.umass.edu/courses/fall2011/biol/biol523/content/elastic-arteries-0 http://bcrc.bio.umass.edu/histology/?q=node/654&size=_original

9 - In: Neurology 2006;67:1809-1812. Mokri B. (1997). "Spontaneous dissections of internal carotid arteries". *Neurologist* **3** (2): 104–119.

10 - Mengyan Li, Mark J. Mondrinos, Milind R. Gandhi, Frank K. Ko, Anthony S. Weiss, Peter I. Lelkes, Electrospun protein fibers as matrices for tissue engineering, Biomaterials, Volume 26, Issue 30, October 2005, Pages 5999-6008

11 - Photograph by Robert Lamberts at The New Zealand Institute for Plant and Food Research Ltd (Wikimedia Commons - http://en.wikipedia.org/wiki/File:Taylor_cone_photo.jpg)

12 - Cylinder stresses. (2012, July 19). In *Wikipedia, The Free Encyclopedia*. Retrieved 17:26, August 8, 2012, from http://en.wikipedia.org/w/index.php?title=Cylinder_stresses&oldid=503084721

## Vita

Casey Grey was born on November 7, 1985 in Augusta, Georgia. He received his Bachelor of Science degree in Mechanical Engineering from the Virginia Military Institute in 2007. After three years as an Assistant Project Manager at Southern Air, Casey returned to graduate school at Virginia Commonwealth University in August, 2010. During his time at VCU, Casey was actively involved in the development of intellectual property in the fields of tissue engineering, mechanical design, and medical device design. He will earn his Master's of Science degree in Biomedical Engineering August, 2012 from VCU.